

We are IntechOpen, the world's leading publisher of Open Access books Built by scientists, for scientists

6,900

Open access books available

186,000

International authors and editors

200M

Downloads

Our authors are among the

154

Countries delivered to

TOP 1%

most cited scientists

12.2%

Contributors from top 500 universities



WEB OF SCIENCE™

Selection of our books indexed in the Book Citation Index
in Web of Science™ Core Collection (BKCI)

Interested in publishing with us?
Contact book.department@intechopen.com

Numbers displayed above are based on latest data collected.
For more information visit www.intechopen.com



Earthquake Induced a Chain Disasters

Guangqi Chen, Yange Li, Yingbin Zhang and Jian Wu
*Kyushu University
 Japan*

1. Introduction

A strong earthquake not only cause directly damage on constructs but also can result in a series of natural disasters such as landslide, debris flow and flooding. These secondary disasters occurs as a chain disasters as shown in Fig. 1. A strong earthquake can induce a large amount of landslides. And then, a large scale landslide can create a landslide dam when its debris fill into and stop a river. The water impounded by a landslide dam may create a dam reservoir (lake). While the dam is being filled, the surrounding groundwater level rises and causes back-flooding (upstream flooding). And because of its rather loose nature and absence of controlled spillway, a landslide dam is easy to fail catastrophically

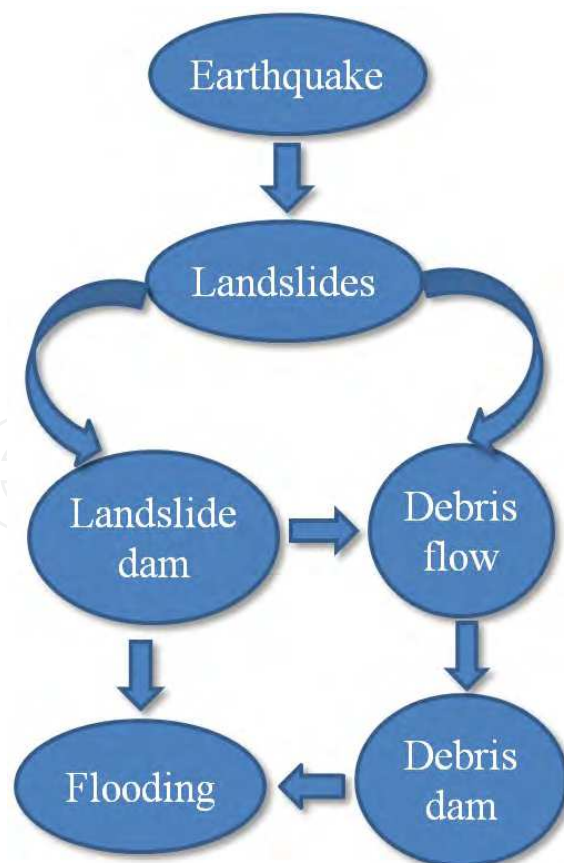


Fig. 1. The disasters chain induced by an earthquake

and lead to debris flow or downstream flooding. Also, since the landslide debris can be removed into a valley or a ravine by excessive precipitation, it is easy to form debris flow, and then create a debris dam sometimes.

In this chapter, we take the 2008 Wenchuan Earthquake ($M_s=8.0$) as an example to discuss the earthquake induced chain disasters. The characteristics of the earthquake induced landslides are summarized including the discussion of the landslide dams. A landslide susceptibility analysis is carried out and a possible long run-out mechanism is proposed for the study. The characteristics of the debris flows arising from the earthquake are summarized. An approach of simulating debris flow is proposed for predicting the movement behaviours of potential debris flow arising from earthquake. A practical simulation is carried out for verifying the approach.

2. The earthquake induced landslide

A strong earthquake can induce a large amount of landslides and cause very serious property damage and human casualties. This phenomenon was recorded in ancient China dated back to 1789 BCE, and in ancient Greece 2373 years ago (Keefer, 2002). There have been many reports about the very serious damages caused by the earthquake induced landslides for the last few decades. For example, 9,272 landslides induced by the 1999 Chi-Chi earthquake ($M_s=7.6$) caused 2,400 deaths, more than 8000 casualties and over 10 billion US\$ of economical loss in Taiwan (Chang et al. 2005). 30% of the total fatalities (officially 87,350) had been victims of co-seismic landslides due to the Kashmir earthquake ($M_s=7.6$) (Havenith and Boureau 2010). In this chapter, we take the 2008 Wenchuan Earthquake ($M_s=8.0$) as example to discuss this issue.

2.1 The 2008 wenchuan earthquake

The earthquake had a magnitude of 7.9 M_s , occurred in Sichuan Province, China at 14:28 CST on 12 May 2008. The epicenter is located Yingxiu town (30.986°N , 103.364°E), Wenchuan County. The focal depth is about 12 km according to the report by the China Earthquake Administration (CEA).

The earthquake occurred along the Longmenshan fault (LMSF) zone at eastern margin of the Tibetan Plateau, adjacent to the Sichuan Basin as shown in Fig. 2 (Gorum et al., 2011). The fault belt is a series of faults striking in a northeast direction, on a North-South zone of high topographical and geophysical gradients between the Tibet Plateau on its western side and the Yangzi Platform on its eastern side. Seismic activities concentrated on its mid-fracture (known as Yingxiu-Beichuan fracture). Starting from Yingxiu, the rupture propagated unilaterally towards the northeast at an average speed of 3.1 kilometers per second, generating a 300-km and a 100-km long surface rupture along the Yingxiu-Berchuan and Pengguan faults, respectively (Huang et al., 2011a). The duration was as long as 120 seconds and the maximum displacement amounted to 9 meters.

Official figures, released by China News www.chinanews.com, on July 21, 2008 12:00 CST show that 69,197 are confirmed dead, 374,176 injured, and 18,222 listed as missing. The earthquake destroyed 5,362,500 and seriously damaged 21,426,600 houses, left about 4.8 million people homeless (Cui et al., 2009, Tang et al., 2011b). Approximately 15 million people lived in the affected area. It was the deadliest earthquake to hit China since the 1976 Tangshan earthquake, which killed at least 240,000 people.

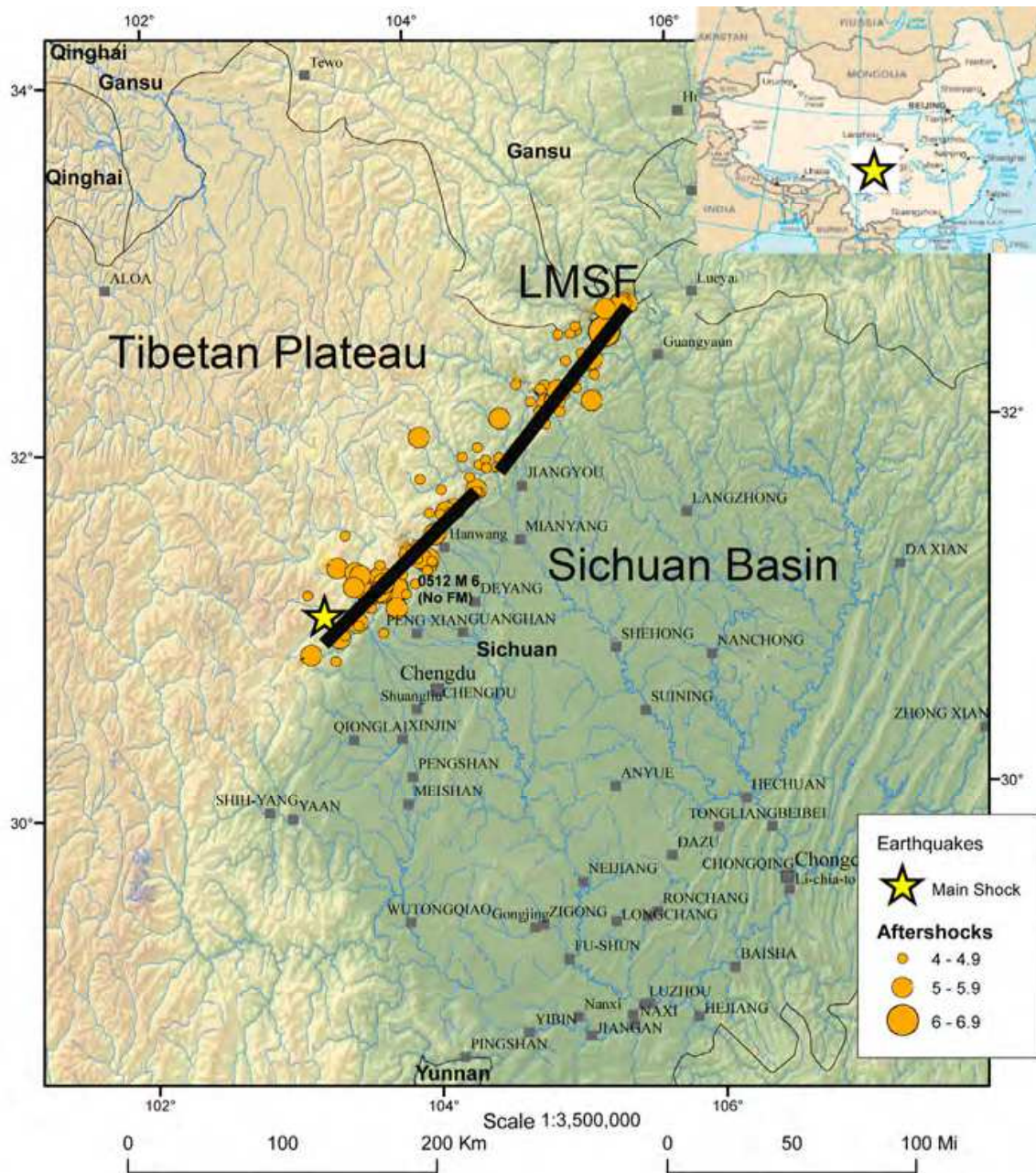


Fig. 2. The 2008 Wenchuan earthquake, LMSF and aftershocks. (modified from United States Geological Survey [USGS], 2008)

2.2 The landslides induced by the earthquake

The earthquake occurred in a mountainous region, where the geological and topographical features and climate conditions are very complex. The response to the ground shock was very strong. The recorded peak ground acceleration of local site reached to 2.0g (Huang et al., 2011b). Because of the complex terrain and climate conditions, the quake induced as many as 56,000 landslides (Dai et al., 2011). It is estimated that over one third of the total lost from the 2008 Wenchuan earthquake was caused by the earthquake induced landslides. Therefore, the secondary chain disaster induced by the 2008 Wenchuan earthquake is much more serious than the 1976 Tangshan earthquake.

2.3 Characteristics of the landslides

As many as 56,000 landslides have been identified by field investigations and using remote sensing technique with aerial photographs and satellite images. And the following distinctive characteristics can be summarized from these landslides:

1. Large scale

Many large scale landslides were induced by the 2008 Wenchuan earthquake. There are tens of landslides with a volume of 10^7 cubic meters (Wu et al., 2010), and 113 landslides with the area larger than 50,000 m² as shown in Table 1 (data from Xu et al., 2009a). The largest one is the Daguangbao landslide in Anxian County with an area of 7,273,719 m² and the volume of about 8.4×10^8 m³ (Chigira et al., 2010).

2. The effect from the hanging and foot wall of the fault

It has been found that the majority of landslides are distributed in the range belonging to the hanging wall of the Yingxiu-Beichuan fault and Pengguan fault, northwest part of earthquake zone. All statistics seem to support that the landslide in hanging wall area is more active than in foot wall areas (Xu et al., 2009a; Yin et al., 2009a). For example, the distribution of large-scale landslides also shows the hanging /foot wall effect. It can be found from the Table 1 that 80 landslides occurred in the hanging wall, 70.8% of the total 113 large-scale landslides, and only 33 landslides occurred in the foot wall, 29.2% of the total number.

No.	Name	Place	Area /m ²	Distance to fault /m	Wall location
1	Daguangbao	Anxian	7,273,719	4,800	Hanging wall
2	Wenjiagou	Mianzhu	2,945,520	3,900	Foot wall
3	Donghekou	Qiangchuan	1,283,627	300	Hanging wall
4	Zhengjiashan	Pingwu	1,014,987	2,400	Hanging wall
5	Shuimogou	Shifang	915,608	700	Hanging wall
6	Dawuji	Anxian	792,190	6,900	Hanging wall
7	Woqian	Qiangchuan	695,672	200	Hanging wall
8	Dashanshu	Mianzhu	693,687	6,900	Hanging wall
9	Hongshigou	Anxian	687,520	2,240	Hanging wall
10	bingkoushi	Pengzhou	575,556	12,600	Hanging wall
11	Tangjiashan	Beichuan	572,009	2,780	Hanging wall
12	Huatizigou	Pengzhou	541,193	4,980	Hanging wall
13	Wenjiaba	Pingwu	537,101	380	Hanging wall
14	Niujuangou	Wenchuan	527,700	300	Hanging wall
15	Haixingou	Mianzhu	517,573	8,888	Hanging wall
16	Ma'anshi	Pingwu	509,836	4,200	Hanging wall
17	Shibangou 1#	Qiangchuan	496,983	2,300	Hanging wall
18	Guershan	Beichuan	471,112	0	Hanging wall
19	Xiaojiashan	Mianzhu	465,899	2,900	Hanging wall
20	Xinkaidong	Pengzhou	449,685	6,800	Hanging wall
21	Bozangcun	Anxian	418,744	4,030	Hanging wall
22	Mianjiaoping	Beichuan	377,247	550	Foot wall
23	Weijiashan	Beichuan	358,021	2,120	Hanging wall
24	Liqigou	Jiangyou	355,113	10,000	Foot wall

No.	Name	Place	Area /m ²	Distance to fault /m	Wall location
25	Caocaoping	Anxian	354,046	660	Hanging wall
26	Miepengzi 3 [#]	Mianzhu	353,817	600	Hanging wall
27	Laoyinggou	Anxian	353,242	1,050	Hanging wall
28	Huoshigou	Anxian	322,155	1,400	Hanging wall
29	Zhangjiashan	Anxian	306,576	6,000	Foot wall
30	Macaotan	Mianzhu	305,989	2,700	Foot wall
31	Xiejiadianzi	Pengzhou	294,256	1,100	Hanging wall
32	Shibangou 2 [#]	Qiangchuan	288,305	2,400	Hanging wall
33	Huishuituo	Pengzhou	270,980	4,200	Hanging wall
34	Dazhuping	Anxian	270,692	540	Hanging wall
35	Miepengzi 2 [#]	Mianzhu	262,520	600	Hanging wall
36	Heshangqiao 3 [#]	Dujaiingyan	257,635	10,400	Hanging wall
37	Muguapingcun	Shifang	256,340	900	Foot wall
38	Miepengzi 1 [#]	Mianzhu	255,296	600	Hanging wall
39	Dongxigou	Beichuan	246,020	2,200	Hanging wall
40	Yaozigou	Pingwu	242,553	800	Hanging wall
41	Baichaping	Dujaiingyan	241,874	4,700	Hanging wall
42	Changping	Pengzhou	224,645	2,400	Hanging wall
43	Baodili	Qiangchuan	222,157	700	Hanging wall
44	Xiaomuling	Mianzhu	218,705	2,450	Hanging wall
45	Heshangqiao 1 [#]	Dujaiingyan	214,020	10,900	Hanging wall
46	Baishuling	Beichuan	208,968	4,350	Hanging wall
47	Dawan	Beichuan	203,959	2,150	Hanging wall
48	Baiguoshu	Beichuan	203,246	1,000	Hanging wall
49	Zengjiashan	Mianzhu	198,165	11,350	Foot wall
50	Zhangjiagou	Beichuan	196,299	640	Hanging wall
51	Zhaojiaqu	Qiangchuan	193,153	1,300	Hanging wall
52	Heitanzi	Anxian	182,452	8,900	Foot wall
53	Anleshan	Beichuan	180,809	1,140	Hanging wall
54	Yangshangou	Beichuan	177,361	1,300	Hanging wall
55	Xiaotianchi	Mianzhu	175,758	8,200	Foot wall
56	Yanyangcun	Beichuan	174,008	1,600	Foot wall
57	Shicouzi	Pingwu	169,540	0	Hanging wall
58	Chenjiaping	Anxian	169,368	1,050	Hanging wall
59	Wangyemiao	Dujaiingyan	167,980	9,300	Hanging wall
60	Jiadanwan 1 [#]	Dujaiingyan	166,643	7,900	Hanging wall
61	Jinhelingkuang	Mianzhu	159,848	2,800	Foot wall
62	Fengyanzi	Beichuan	158,468	0	Foot wall
63	Changtan	Mianzhu	151,094	6,670	Foot wall
64	Weijiagou	Beichuan	150,818	450	Hanging wall
65	Xiaogangjian	Mianzhu	149,074	6,280	Foot wall
66	Baiyanshan	Qiangchuan	147,940	4,300	Hanging wall
67	Guoniucun	Beichuan	147,554	3,000	Hanging wall
68	Heshangqiao 2 [#]	Dujaiingyan	147,394	9,600	Hanging wall
69	Bazuofen	Anxian	146,272	11,000	Foot wall
70	Tiangengli	Qiangchuan	144,729	1,400	Foot wall

No.	Name	Place	Area /m ²	Distance to fault /m	Wall location
71	Hongmagong	Qiangchuan	144,683	350	Foot wall
72	Baiguocun	Qiangchuan	139,800	300	Foot wall
73	Huangtuliang	Beichuan	135,084	550	Hanging wall
74	Qinglongcun	Qiangchuan	134,079	790	Foot wall
75	Pengjiashan	Beichuan	127,156	2,900	Hanging wall
76	Wangjiayan	Beichuan	125,381	400	Hanging wall
77	Yibadao	Mianzhu	125,059	9,600	Foot wall
78	Laohuzui	Wenchuan	125,039	2,700	Hanging wall
79	Beichuanzhongxuexinqu	Beichuan	124,365	300	Foot wall
80	Xiaomeizilin	Mianzhu	122,530	5,800	Foot wall
81	Xiangshuishi	Pengzhou	119,194	4,600	Hanging wall
82	Gaojiamo	Pingwu	115,301	1,600	Hanging wall
83	Jiadanwan 2 [#]	Dujaingyan	114,905	9,300	Hanging wall
84	Dahuashu	Beichuan	113,111	0	Hanging wall
85	Wangjiabao	Beichuan	112,418	0	Hanging wall
86	Jiankangcun	Pingwu	111,106	340	Hanging wall
87	Xiaojiaqiao	Anxian	110,085	3,000	Foot wall
88	Lingtou	Qiangchuan	102,116	800	Hanging wall
89	Longwangou	Beichuan	99,821	650	Hanging wall
90	Zhangzhengbo	Qiangchuan	99,726	790	Foot wall
91	Nanyuecun	Dujaingyan	99,350	0	Hanging wall
92	Hongkouxiangxiajiaping	Dujaingyan	96,345	790	Hanging wall
93	Dujiayan	Qiangchuan	94,769	960	Foot wall
94	Madiping	Qiangchuan	94,633	2,600	Hanging wall
95	Maochongshan 1 [#]	Pingwu	92,355	1,200	Hanging wall
96	Yandiaowo	Qiangchuan	92,128	340	Foot wall
97	Chuangzigou	Mianzhu	91,718	2,200	Foot wall
98	Xiaoxishan	Qiangchuan	90,298	1,000	Hanging wall
99	Xishanpo	Beichuan	83,663	1,140	Hanging wall
100	Hejiayuan	Qiangchuan	83,359	1,990	Foot wall
101	Zhaojiashan	Qiangchuan	82,329	1,000	Foot wall
102	Liushuping 1 [#]	Qiangchuan	81,000	780	Hanging wall
103	Weiziping	Qiangchuan	74,661	470	Hanging wall
104	Gongziba	Qiangchuan	71,221	220	Hanging wall
105	Maerping	Qiangchuan	70,982	7,500	Hanging wall
106	Maochongshan 2 [#]	Pingwu	70,252	1,200	Hanging wall
107	Muhongping	Qiangchuan	68,288	2,600	Foot wall
108	Machigai	Qiangchuan	66,602	500	Foot wall
109	Zixicun	Pingwu	57,820	2,400	Hanging wall
110	Liushuping 2 [#]	Qiangchuan	54,810	1,000	Hanging wall
111	Dongjia	Qiangchuan	54,353	1,000	Foot wall
112	Majiawo	Qiangchuan	50,591	1,100	Hanging wall
113	Xiaowuji	Qiangchuan	50,122	2,100	Foot wall

Table 1. The large scale landslides with the area larger than 50,000 m² (data from Xu et al., 2009a).

3. The effect from the distance to the faults

Among the large scale landslides, the two farthest landslides from the fault are about 12.6km in the side of hanging wall and 11.35km in the foot wall. The majority of landslides (about 70%) occurred in the region of 3km from the fault. Fig. 3a and 3b show the accumulative percentage of landslide distribution as a function of the distance to the fault in hanging and foot wall respectively. An exponential decay has been found for the number of landslides with the distance to the fault in both hanging and foot wall (Fig. 4).

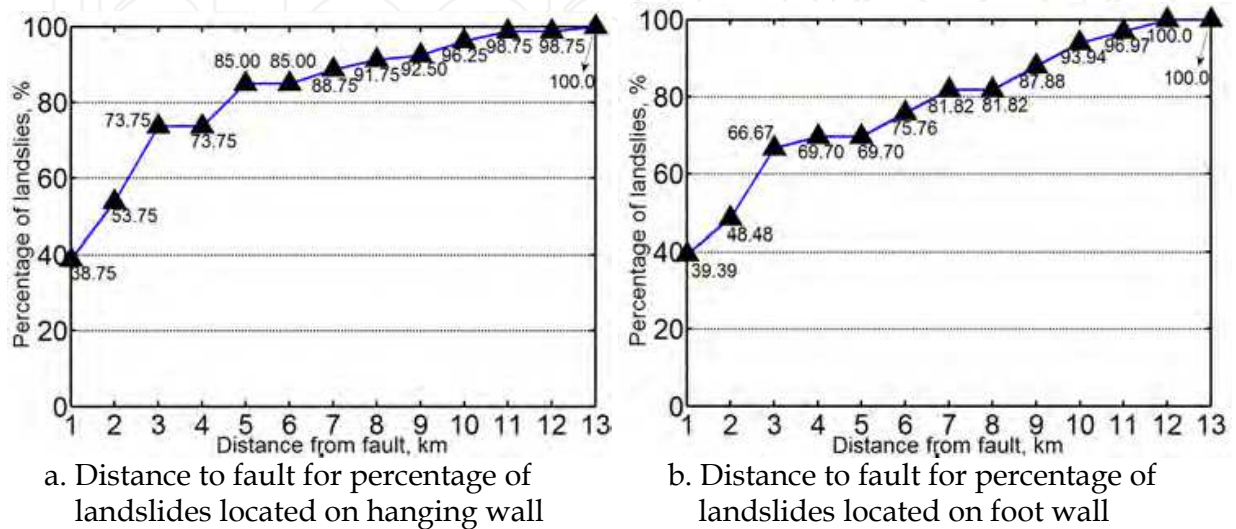


Fig. 3. Relationship between percentage of landslides and large-scale distance to fault. a: Distance to fault for percentage of landslides located on hanging wall; b: Distance to fault for percentage of landslides located on foot wall.

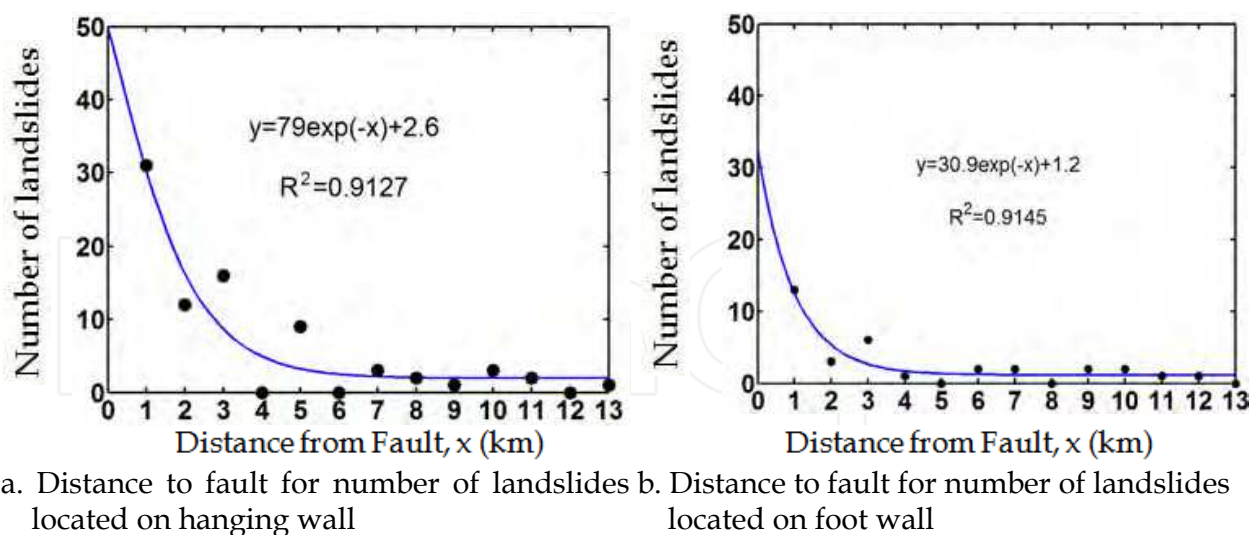


Fig. 4. Relationship between number of landslides and distance to fault. a: Distance to fault for number of landslides located on hanging wall; b: Distance to fault for number of landslides located on foot wall.

4. Effect from the locking segment of the fault zone

The two largest scale landslides: Daguangbao landslide with the area of 7,273,719m² and Wenjiagou landslide with the area of 2,945,520m² are found locating at a distance of more

than 3.9km from the fault from Table 1, although most of large-scale landslides, which many researchers have been studying on, are located in the region of less than 1km from the fault. For example, the Donghekou landslide (No.3 in Table 1) has a distance of 0.3km, the Woqian landslide (No.7 in Table 1) has a distance of 0.2km and Niujuangou landslide (No.14 in Table 1) has a distance of 0.3km from the fault. By examining the positions of the two landslides with the fault zone, it has be found that the two landslides are just located at the locking segment of the fault zone where high stress is believed to be concentrated and a lot of energy was absorbed by the locking of the rupture fault. Therefore, it should be notice that large scale landslides may occur at such kind of locking segment of the fault zone.

5. Direction effect

By examining the sliding directions of large-scale landslides along Hongshihe valley, it has been found that the directions parallel to or perpendicular to the fault are dominated as shown by the rose diagram in Fig. 5. It is implied that the landslides are controlled by the earthquake wave propagation and the fault movement. The slopes parallel to or perpendicular to the fault are easy collapsed.

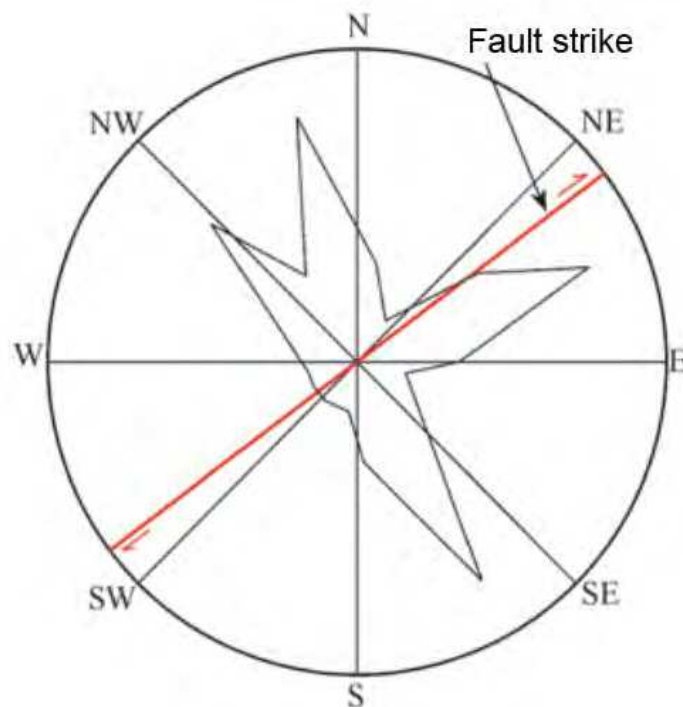


Fig. 5. Rose diagram showing the motion direction of large-scale landslides along the Hongshihe (after Xu et al., 2009a)

6. The long run-out characteristic

For rainfall induced landslides, the run-out distances are mostly less than 2 times of the slope height ($2H$). For example, 95% of the 19,035 landslides induced by rainfall are less than 50m based on the records from 1972 to 2008 in Japan. However, numerous rapid and long run-out landslides occurred during the 2008 Wenchuan Earthquake. Table 2 lists 21 long-run-out landslides with the horizontal distance larger than 500m. These landslides traveled over extraordinarily large distances with extremely high speeds and produced catastrophic results.

For instance, the Wangjiayan landslide (No. 76 in Table 1 and No. 21 in Table 2), occurred at the old town area of Beichuan city, had a run-out distance of 550m. It destroyed hundreds of buildings and resulted in more than 1600 fatalities (Yin et al., 2009a). The Daguangbao landslide (No. 1 in both Table 1 and 2) is another long run-out example. The affected area is estimated more than 7.2 km². Its run-out distance is estimated as 4,500m. The most complex in dynamic mechanism is the Donghekou landslide (No. 3 in Table 1 and No. 4 in Table 2) which has the run-out distance of over 2.4km. It blocked two rivers and formed two landslide lakes at Donghe village of Qingchuan County.

It has been found that the run-out distance is proportional to the area and volume of landslide. The regression formulas of $D/H = \lg S - 3.12$ has been obtained with a coefficient of determination of $R^2 = 0.7681$, where D is the run-out distance, H is the slope height and S is the area of landslide. and $D/H = 0.54 \lg V - 1.26$ with a coefficient of determination of $R^2 = 0.6290$, where V is the volume of landslide (see Fig. 6).

Since the mechanism of long run-out landslide is very important in landslide disaster mitigation, it will be discussed in Section 4.

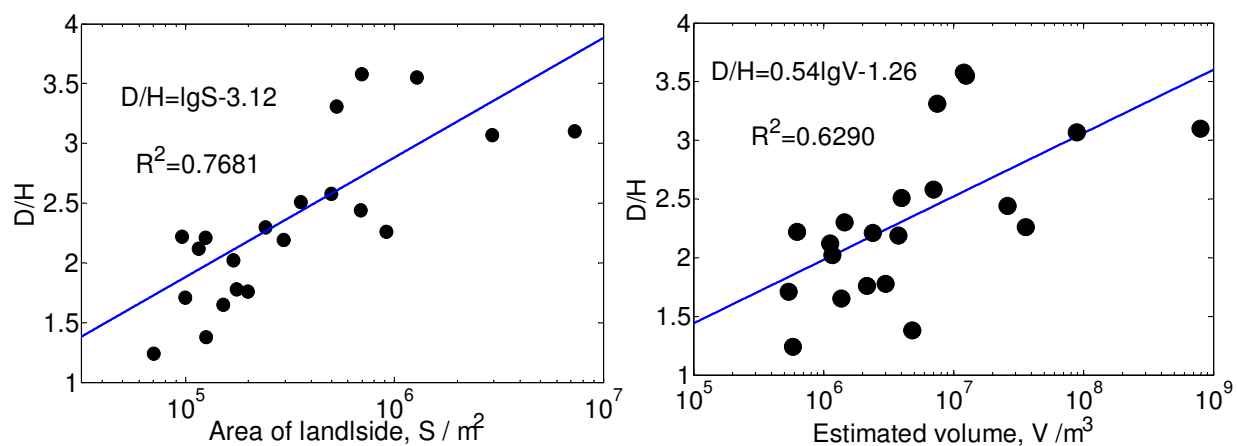


Fig. 6. The relationship between normalized run-out distance and (a) the area of landslide, S (m²), and (b) the volume of landslide, V (m³).

7. Large number of landslide dams

There are 34 landslide dams formed by the earthquake induced landslides. These landslide dams blocked the major large rivers. The water impounded by landslide dams created dam lakes.

The largest scale landslide dam was formed by the Tangjiashan landslide. It blocked the upper portion of the Jianjiang River at a location of about 5 km from Beichuan County Town. The dam crest extended approximately 600 m across and 800 m along the valley (Xu et al., 2009b). The maximum height of the dam is about 124 m. The maximum capacity of the landslide lake was $2.4 \times 10^8 \text{ m}^3$, with the length of 20 km (Yin et al., 2009a).

Because of its rather loose nature and absence of controlled spillway, it is feared that the landslide dam may fail catastrophically and lead to downstream flooding with high casualties. Hundreds of thousands of residents in downstream Mianyang City were evacuated to the higher locations out of the town before a temporary drainage channel was dugged in the dam by Chinese government.

Rank	No. in Table 1	Name	Place	Area/m ²	Distance from fault/m	Estimated Volume/m ³	Height H/m	I
1	1	Daguangbao	Anxian	7,273,719	4,800	7.5×10 ⁸ *-8.4×10 ⁸ ®	≈1450*	
2	2	Wenjiagou	Mianzhu	2,945,520	3,900	2.75×10 ⁷ -1.5×10 ⁸ *	1,360	
3	14	Niujuangou	Wenchuan	527,700	300	7,500,000	827	2
4	3	Donghekou	Qiangchuan	1,283,627	300	1.0×10 ⁷ ⊙-1.5×10 ⁷	680	
5	24	Liqigou	Jiangyou	355,113	10,000	4,000,000	920	
6	9	Hongshigou	Anxian	687,520	2,240	26,000,000♥	≈900*	
7	5	Shuimogou	Shifang	915,608	700	36,000,000♥	≈930*	
8	7	Woqian	Qiangchuan	695,672	200	12,000,000	570	
9	17	Shibangou 1#	Qiangchuan	496,983	2,300	7,000,000	710	1
10	31	Xiejadianzi	Pengzhou	294,256	1,100	3.5×10 ⁶ -4.0×10 ⁶ ⊙	740	1
11	58	Chenjiaping	Anxian	169,368	1,050	1,163,446	680	
12	41	Baichaping	Dujaingyan	241,874	4,700	1,449,340	580	
13	63	Changtan	Mianzhu	151,094	6,670	1,367,868	800	
14	49	Zengjiashan	Mianzhu	198,165	11,350	2,166,334	700	
15	55	Xiaotianchi	Mianzhu	175,758	8,200	2,999,540	630	
16	89	Longwangou	Beichuan	99,821	650	540,382	520	
17	82	Gaojiamo	Pingwu	115,301	1,600	1,126,823	340	
18	92	Hongkouxiangxiajiaping	Dujaingyan	96,345	790	624,296	300	
19	79	Beichuanzhongxuexinqu	Beichuan	124,365	300	2,400,000⊙	≈300*	
20	106	Maochongshan 2#	Pingwu	70,252	1,200	581,719	490	
21	76	Wangjiayan	Beichuan	125,381	400	4,800,000⊙	≈400*	

Note: * data from Huang et al. (2011a); ♥ data from Wu et al. (2010); ♦ data from Qi et al. (2011); ® data from Yin et al.(2009a); ⊙ Estimated indirectly from geological sections or description.
 ° notes the value is mean one if the number of data more than one.

Table 2. Some long run-out landslides triggered by the Wenchuan earthquake (arranged from the H from Xu et al., 2009a)

IntechOpen

3. Susceptibility analysis of earthquake induced Landslides

Landslide susceptibility analysis (LSA) is necessary and important for land use planning and disaster mitigation. Many researchers have made great effort to identify the relationships of landslide characteristics such as distribution pattern, type, area coverage and volume with the triggering factors such as the magnitude, intensity and peak ground acceleration (PGA) of the earthquake, coseismic fault rupture (e.g. Lee et al., 2008; Rodriguez et al., 1999; Miles and Keefer, 2009; Keefer, 1984, 2000, 2002; Papadopoulos and Plessa, 2000). Some researchers have studied the relationships of landslide distribution with geo-environmental factors such as lithology, morphology, presence of secondary active or inactive faults (e.g. Chigira and Yagi, 2006; Jibson et al., 2000; Khazai and Sitar, 2003; Keefer, 2000; Yagi et al., 2009).

The Wenchuan earthquake induced landslides has been carried out by several researchers. For example, Huang et al. (2011a) studied the characteristics and failure mechanism of Daguangbao Landslide, the largest scale landslide, and suggested a classification system. Tang et al. (2011b) studied the effect of the quake on the landslides induced by the subsequent strong rainfall after earthquake by a case study in the Beichuan area. Qi et al. (2010) built a spatial database of landslides by using the remote sensing (RS) results which cover 11 counties seriously damaged by the earthquake. Yin et al (2009a, b) analyzed the landslide distribution, the mechanisms of some typical landslides, and evaluated the potential hazards of the landslide dams. Gorum et al. (2011) presented the preliminary results of an extensive study of the mapping the distribution of landslides by using a large set of optical high resolution satellite images. Yin et al. (2010) presented a quantitative result of the number and area of the landslides from Anxian to Beichuan. Dai et al. (2011) mapped over 56,000 landslides using aerial photographs and satellite images and characterized the spatial distribution of landslides by correlating landslide-point density and landslide-area density with the physical parameters that control the seismic stability of slopes.

In this chapter, we show some results from landslide susceptibility analysis carried out in Qingchuan County. Our analysis was based on slope units rather than the traditional grid units. At first, the relationship of landslide distribution with an individual causative factor is analyzed. And then, landslide susceptibility is analyzed by using artificial neural network (ANN) method. Finally, a landslide susceptibility map is made based on the ANN results.

3.1 Study area and data source

Qingchuan County is located at the north-western part of the earthquake zone as shown in Fig. 7. The landslides in the area of 3,271km² are studied.

3.2 Slope unit

Up to now, most of such studies were carried out based on the grid units. There is a problem in grid-based study that a grid may contain different slopes and a large slope may contain several grids with different slope grades. Despite the problem, the grid units were still used just because the slope units are difficult to be indentified for a wide range in the past.

Nowadays, it becomes possible and easy to indentify slope units by using GIS-based hydrologic analysis tool (David, 2002), which is based on the watershed divide and drainage lines. The slope unit size should be determined when the tool is used. We suggest that the appropriate slope unit size should match the average size of the landslide bodies in the study area.

A total of 55,899 slope units were indentified in Qingchuan County (Fig. 8). They will be used for landslide susceptible analysis in this study.

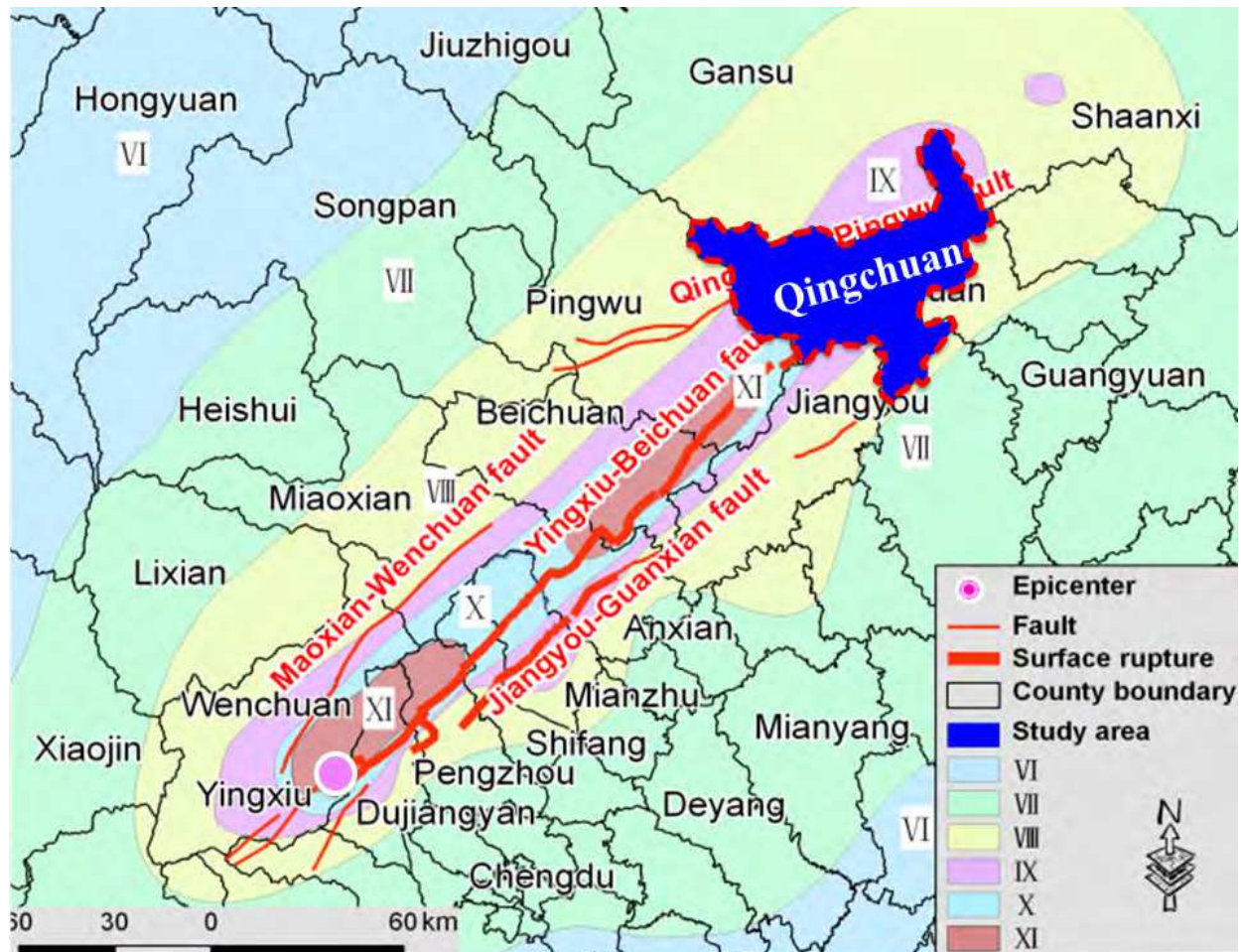


Fig. 7. Location of the study area

The basic data include a 1:100,000 geological map and a 10m grid digital elevation model (DEM) made from the available topographic map with 5m contour line interval. 885 landslides were identified from field investigations and RS results.

3.3 Relationship between landslide and individual causative factor

More than fifty factors can be considered as the landslide causative factors (Lin, 2003). By considering the data availability, analysis effectiveness, and independence of each factor (Lee et al., 2008), we selected the follow 8 factors: slope gradient, elevation, slope range, slope aspect, specific catchment area, lithology, distance to the fault and distance to the stream, to examine the causative factors contributing to the initiation of landslides.

Each causative factor was classified into several categories. The number of the slope units in each category is calculated and the percentage of the category among the whole slopes is given in Fig.9(b). For each category, the percentage of the failure slopes among the slopes in the same category is given as the landslide frequency in Fig. 9(a).

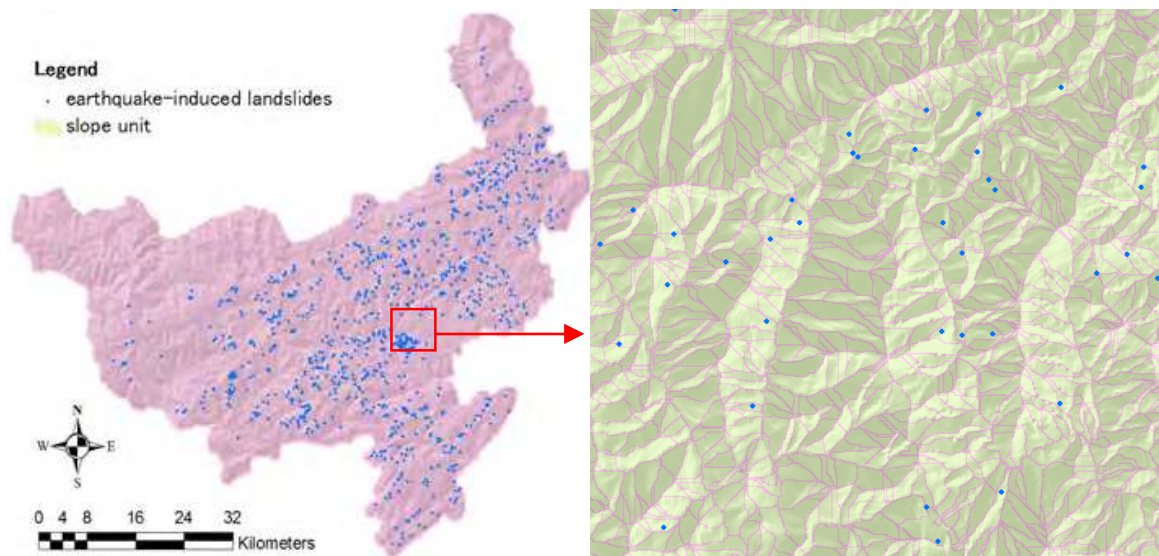


Fig. 8. Slope unit division of Qingchuan area

From the statistical analysis, the following results can be found.

1. More than 90% of the slopes have the slope gradient larger than 20° . The landslides occurred majorly in the slopes with gradients between 20° to 35° .
2. The landslides occurred majorly in the area with the elevations less than 1,200m.
3. The landslides occurred majorly in the slopes with slope ranges from 200 to 400m.
4. There is no clear relationship between landslides and specific catchment area.
5. The number of the landslides in the slopes in N direction is as twice as the slopes in the other directions.
6. The number of the landslides in the slopes with the distances to the fault less than 0.5km is as twice as the slopes in other categories.
7. The number of the landslides in the slopes with the distances to a stream less than 5km is as 3 times as the slopes in other categories.
8. There is no clear relationship between landslides and lithology.

3.4 Landslide susceptibility analysis using artificial neural network

The landslide susceptibility analysis is carried out by using artificial neural network (ANN) based on the above statistical analysis results.

ANN program is a "computational mechanism able to acquire, represent, and compute a mapping from one multivariate space of information to another, given a set of data representing that mapping, which is independent of statistical distribution of the data, can resolve the nonlinear problem and get high prediction accuracy for classification problem especially for large amount samples (Garrett, 1994). The applications of ANN to landslide susceptibility evaluation have been made by many researchers (e.g. Ermini, L., et al., 2005; S. Lee et al., 2006; Pradhan, B et al., 2010). Nefesilioglu et al. (2008) showed that ANN could give a more optimistic evaluation of landslide susceptibility than logistic regression analysis. Ermini et al. (2005) compared two neural architectures: probabilistic neural network and multi-layered perceptron, and obtained a better prediction result.

In this study, the neural network tool SPSS clementine is used since very few parameters are required. One group of the total slopes are randomly selected for training. 611 collapsed slopes of 885 landslides (70%) and 3300 of 55014 un-collapsed slopes (6%) are randomly selected for this group.

Two cases have been analyzed. Case 1 used the 8 factors mentioned as the statistical analysis and Case 2 used the 5 factors, 3 factors with the smaller weight values were removed from the 8 factors. Also, different layers are used for the two cases.

The weights for each factor, experiments structures and the accuracy from the analysis results are shown in Table 3. It can be seen that the accuracy of Case 2 is a little bit higher than Case 1. Therefore, the ANN model from Case 2 is used for the landslide susceptibility classification.

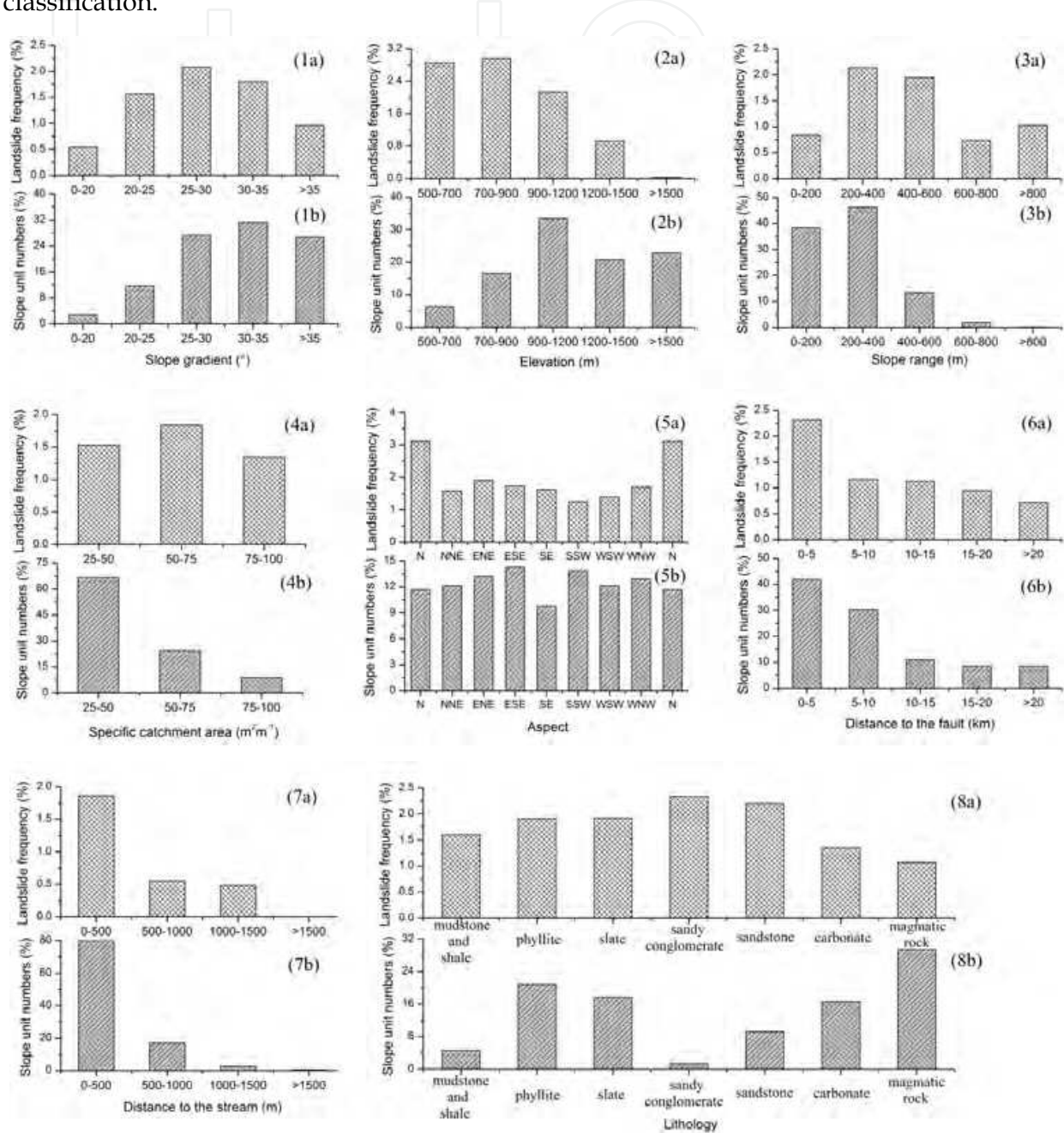


Fig. 9. Landslide frequency and slope unit numbers (%) for each category of causative factor

The output landslide susceptibility indices (LSI) were converted to GIS grid data in three susceptible levels as shown in Table 4. There are 4145 slopes identified as high susceptible level (dangerous slopes), 48,373 slopes identified as low susceptible level (stable slopes), 3,382 slopes identified as medium susceptible level (gray zone).

Causative factors	Case 1	Case 2
Slope gradient	0.367	0.446
Elevation	0.253	0.327
Slope range	0.193	0.163
Aspect	0.038	×
Specific catchment area	0.037	×
Distance to the fault	0.054	0.016
Distance to the stream	0.035	0.048
Lithology	0.023	×
Accuracy	95.05%	96.39%
ANN Structure	8*16*1	5*3*5*1

Table 3. Weight of each factor in 2 cases

By comparing with real landslides, it can be found that 877 of 885 landslides and 3268 stable slopes are identified as high susceptible level, which means 99% of landslides can be predicated by the model but 78.8% of predictions would be false alarm.

On the other hand, 1 of 885 landslides and 48373 stable slopes are identified as low susceptible level, which means 99.4% of predications are correct and less than 0.2% landslides would not be alarmed.

LSI	Susceptible level	Practical		Analysis result	
		Collapsed	Stable	Slope number	(%)
0.0-0.01	Low	1	48372	48373	96.53
0.01-0.1	Medium	7	3375	3382	6.05
0.1-0.9966	High	877	3267	4144	7.42
	Total	885	55014	55899	100.00

Table 4. Characteristics of the three susceptibility zones

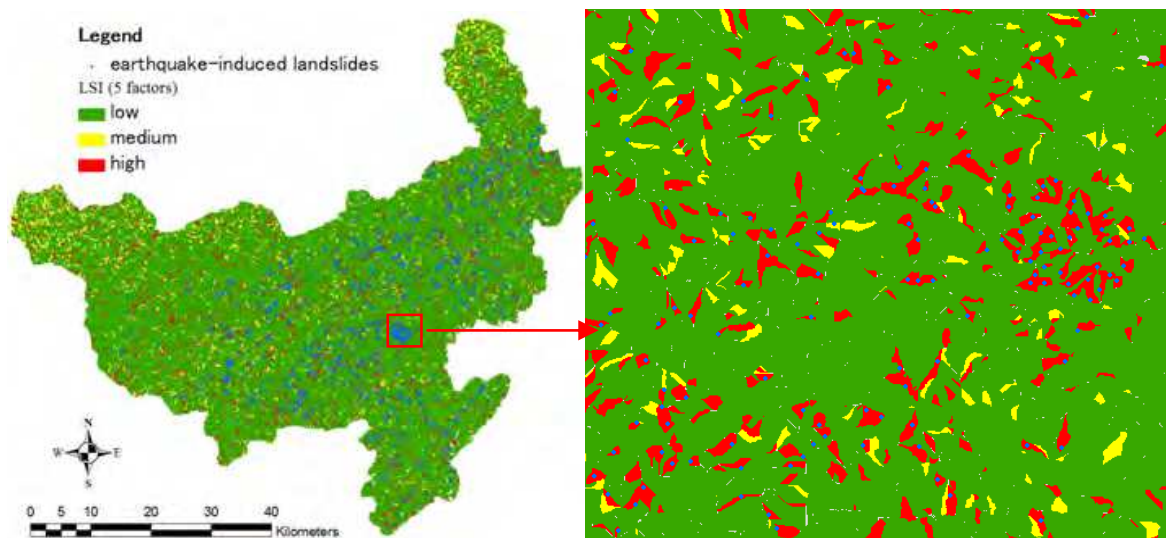


Fig. 10. Earthquake-induced landslide susceptibility map by using ANN analysis.

The landslide susceptibility map is made from the ANN results (Fig. 10). The high susceptible zone occupies 7.42%, the low susceptible zone 86.53% of the whole area. In addition, 6.05% of the area is gray zone.

3.5 Conclusions

Landslide susceptible analysis has been carried out in Qingchuan County. 55,899 slope units have been extracted and used for the analysis. The relationship between landslide distribution and the individual causative factor has been investigated by statistical analysis. The clear relationship can be identified for slope gradient, elevation, slope range, the distances to the fault and the distances to a stream. The ANN analysis also showed the same results, that is, slope gradient, elevation, slope range, distance to the fault and distance to a stream have relatively larger weight. By removing the other three factors with smaller weights, the ANN analysis accuracy got improved. By comparing landslide occurrence locations with susceptibility zones, it has been shown that 99% of landslides can be predicted by the obtained ANN model, but 78.8% of predictions would be false. On the other hand, 99.4% of stable predictions are correct and less than 0.2% landslides would not be alarmed. In addition, the gray zone occupies 6% of the whole area. Therefore, the landslide susceptibility classification presented in this study is acceptable.

4. Analysis of Long run-out mechanism based on trampoline effect

The estimation of the movement behaviour of a potential landslide is very important in order to mitigate the landslide disaster. Especially, the run-out distance is one of the major parameters in landslide risk assessment and preventive measure design. Long run-out is one of the major characteristics of earthquake induced landslides. However its mechanism has not been understood very well.

Many researchers have made great effort to understand how and why large falling masses of rock can move unusually long run-out distance. Researchers have repeatedly revisited the problem using a wide variety of approaches. These efforts have yielded no less than 20 mechanical models for explaining long run-out in high-volume rapid landslides. Shaller and Shaller (1996) made a detail summary of the existed models and divided these models into four categories (1) bulk fluidization and flow of landslide debris; (2) special forms of lubrication along the base of the slides; (3) mass-loss mechanisms coupled with normal frictional sliding; and (4) individual-case mechanisms.

Actually, most of the existed models are helpful in the estimation of the run-out distance. However, very less of them considered the earthquake dynamical behaviour. For this reason, in this study, we take into account the so-called trampoline effect of earthquake on landslides and propose a multiplex acceleration model (MAM) to explain the long run-out mechanism. Since the MAM model can be easily incorporated into numerical methods, it can be applied to simulate the long run-out landslide very well.

4.1 Multiplex acceleration model

For an earthquake induced landslide, the following effects on the movements of the falling stones from the landslide can be considered: (1) a falling stone can obtain kinetic energy

from the colliding with the vibrating slope during earthquake; (2) the force of friction between a falling stone and the slope can decrease since the normal force varies with the contact condition during earthquake; (3) The flying and rotation movement of a falling stone may occur much easily in earthquake induced landslides.

In order to consider these effects, we divide a period of wave is divided into two phases: *P*-phase and *N*-phase as shown in Fig. 11. The *P*-phase is defined as the period when the slope is moving in the outer normal direction of the slope surface. The slope is pushing the falling stones on its surface and lets them obtain kinetic energy in the *P*-phase. The *N*-phase is defined as the period when the slope is moving in the inner normal direction of the slope surface. Since the normal force will decrease when the slope surface moves apart from the falling stones, the force of friction will get decreased in the *P*-phase.

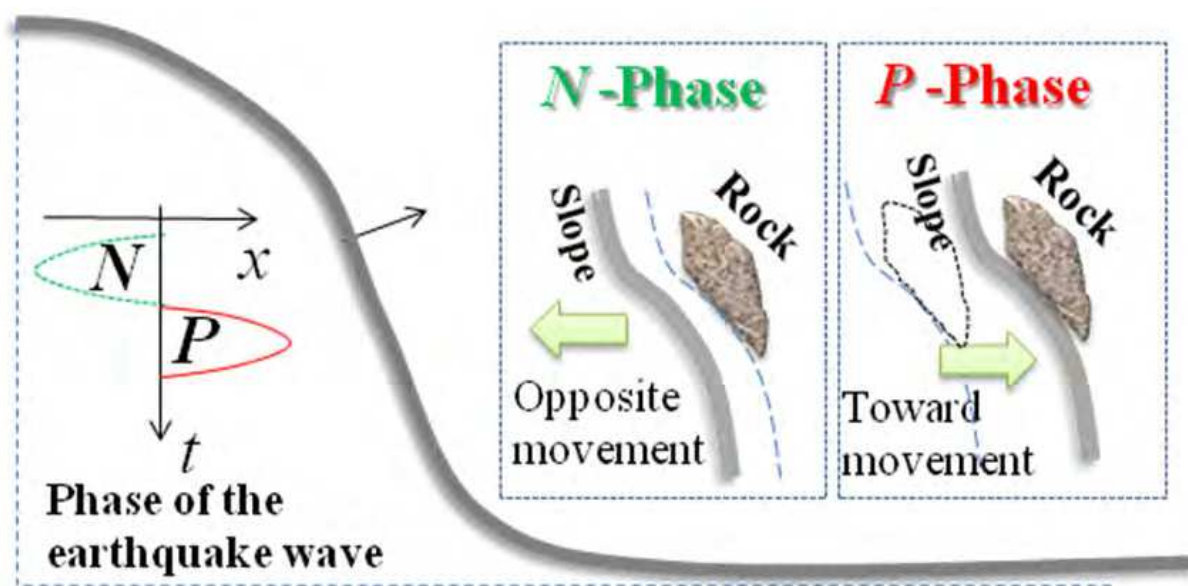


Fig. 11. *P*-phase and *N*-phase definition in MAM

By the repeated exchange of two phases during an earthquake, the falling stone get multiplex accelerated. The MAM model can be seen more clearly by apparent friction angle analysis.

Supposing that a stone with mass m moves from position A to position B during a landslide without earthquake (see Case 1 in Fig. 12), the potential energy decreases by mgh . Based on the energy conservation law, it is easy to obtain the following equation for a falling stone movement in the case without earthquake.

$$mgh - \sum_{i=1}^n l_i mgk_i \tan \varphi_{si} \cos \theta_i = 0 \tag{1}$$

The first term here is for potential energy and the second term is for the work of friction force between the slope and the falling stone, where the sliding movement is considered and the whole curve path is divided into finite linear segments. And m = mass, g = gravity acceleration, h = the falling height, l = the segment length, θ is the segment slope angle, φ is the friction angle, k is the coefficient of conveying from static to dynamic friction and i is the index of segment.

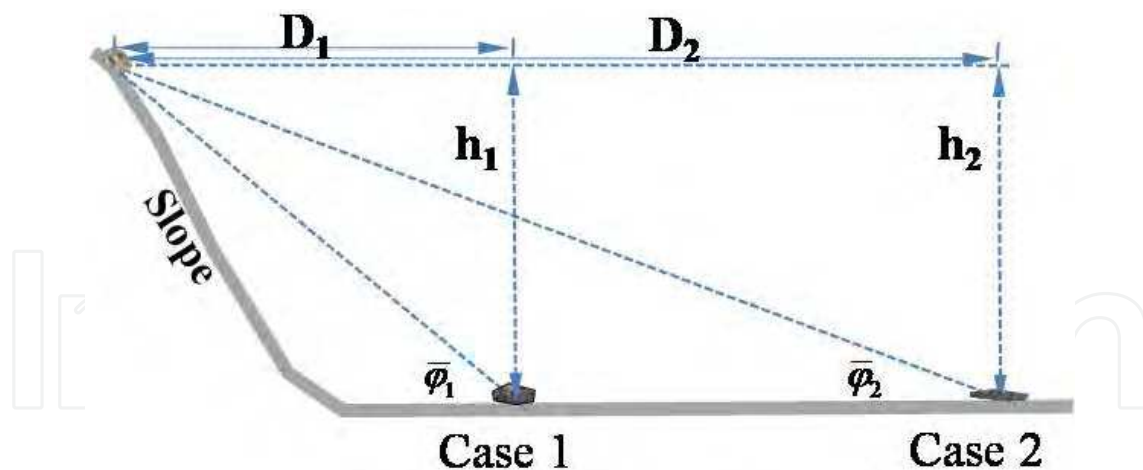


Fig. 12. Apparent friction angle

The apparent friction angle, usually used for the discussion of run-out distance, can be obtained from Eq. (1) as follows

$$\tan \bar{\varphi}_1 = \frac{h_1}{D_1} = \sum_{i=1}^n w_i k_i \tan \varphi_{si} \quad (2)$$

When we consider the effects of slope vibration due to earthquake, the kinetic energy of falling stone obtained from the collision with the vibrating slope and the movement patterns (sliding, rolling and flying) should be considered. Thus, Eq. (1) becomes

$$mgh + \sum_{j=1}^m \frac{1}{2} m v_{ej}^2 - \sum_{i=1}^n l_i m g k_i^* \tan \varphi_{si} \cos \theta_i = 0 \quad (3)$$

The second term here is for the kinetic energy of a falling stone obtained from the collision with the vibrating slope and v_{ej} is the velocity obtained in j^{th} P-phase and can be expressed as follows

$$v_{ej} = VTR \int_{t_j}^{t_j + \Delta t} f(t) dt \quad (4)$$

$f(t)$ is the acceleration of slope vibration due to earthquake, VTR is called the velocity transmission ratio due to collision.

The apparent friction angle for the case 2 in Fig. 12 can be obtained from Eq. (3) as follows

$$\tan \bar{\varphi}_2 = \frac{h_2}{D_2} = \sum_{i=1}^n w_i k_i^* \tan \varphi_{si} - \sum_{j=1}^m \frac{v_{ej}^2}{2gD_2} \quad (5)$$

Comparing Eq.(5) with Eq.(2), it can be seen clearly that the mechanism of long run-out distance is as follows.

1. The kinetic energy of a falling stone obtained from the collision with the vibrating slope may result in long run-out distance from the second term of Eq. (5).
2. The coefficient of conveying from static to dynamic friction k^* in Eq. (5) can be smaller than k in Eq. (3) because of the N -phase effect, air cushion effect, movement pattern.

4.2 Colliding effect

In *P*-phase, a falling stone can obtain kinetic energy from the colliding with the vibrating slope. According to elastic collision theory, when two objects with different masses collide with each other, the object with smaller mass could obtain larger velocity. Since the mass of a slope is much larger than the mass of a falling stone, the velocity of the falling stone can be much larger than the vibrating velocity of the slope. That is to say the *VTR* in Eq. (4) can be larger than 1.0.

The *VTR* can be examined by the simple model shown in Fig. 13(a) and (b). The masses of the two blocks are m_1 and m_2 respectively. Before the colliding, the block 1 has initial velocity V_{10} toward block 2 which is standstill, i.e. $V_{20}=0$. The friction between blocks and the base is negligible. After the colliding, the velocity of block 1 becomes V_{11} while block 2 obtains a velocity V_{21} .

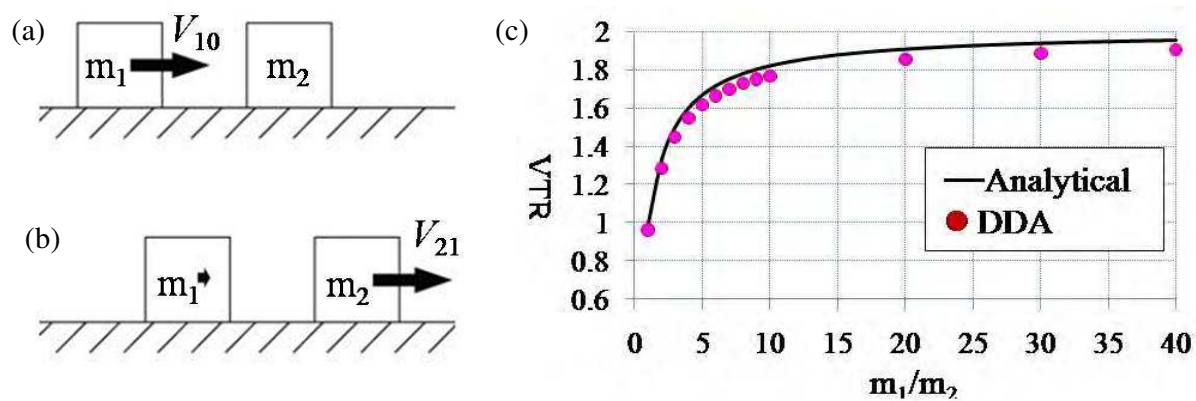


Fig. 13. The colliding model and *VTR* with mass ratio. (a) before the collision, (b) after the collision, (c) *VTR* obtained by DDA comparing with analytical solution.

According to the principles of the conservation of both energy and momentum, we have the following equations.

$$m_1V_{10}^2 + m_2V_{20}^2 = m_1V_{11}^2 + m_2V_{21}^2 \tag{6}$$

$$m_1V_{10} + m_2V_{20} = m_1V_{11} + m_2V_{21} \tag{7}$$

By solving Eqs. (6) and (7), we can obtain the *VTR* for the case of $V_{20}=0$ as follows

$$VTR = 2 \cdot \frac{m_1}{m_1 + m_2} \tag{8}$$

It can be seen from the analytical solution Eq. (8) that if m_1 is much larger than m_2 , *VTR* is to approach to 2.0. Therefore, since the mass of a slope is far larger than the falling stone, the velocity of the falling stone obtained from the slope vibration will be two times of that of the slope vibration velocity during earthquake.

The results of *VTR* given in Eq. (8) have been verified by DDA simulation. The model shown in Fig. 13 is used in DDA simulations. The block one with mass of m_1 has the initial velocity of 10 *m/s* and the block two with mass of m_2 is at a standstill. After the block one impacted the block two, the velocities of both blocks changed. The block two obtained the velocity from block one. The *VTR* is calculated from the ratio of V_{21} to V_{10} .

The results obtained from DDA simulations by changing m_1 are shown in Fig. 13(c), together with the theoretical analytical values. The line is calculated from the analytical solution Eq.(8) and the dots are obtained from DDA simulations.

It can be seen that the *VTR* obtained from DDA is in quite good agreement with the analytical solution. However, by close examination, it can be found that the *VTR* values from DDA are little smaller than the analytical values when the mass ratio of m_1 to m_2 is larger than 4.0. This is because elastic strains of the two blocks are led to energy transformed into potential energy of deformation by the collision in DDA simulation while no strain is considered in analytical solution.

Furthermore, when the block 2 has an initial velocity toward block 1, the *VTR* could become the larger and larger. Fig. 14 shows the results from DDA simulation. This may happen when a stone fall down to the slope in a *P*-phase, it will get larger rebounding velocity. That means, a trampoline effect can be produced by strong earthquake.

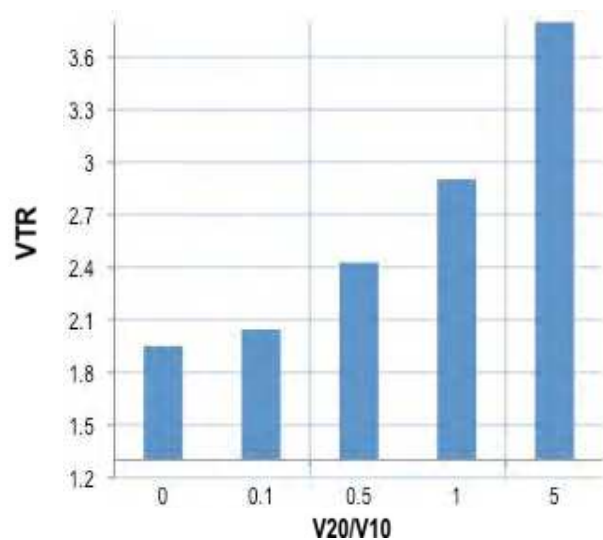


Fig. 14. The *VTR* variation with the initial velocity of block 2

4.3 Model tests by shaking table

Model tests using shaking table were carried out in order to investigate the effects of earthquake on the movement of debris. The model slope has the height of 180cm and the slope angle can be adjusted from 30° to 35° as shown in Fig. 15.

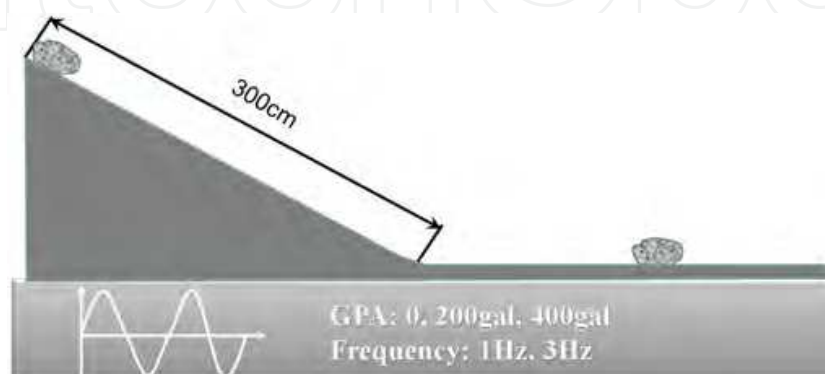


Fig. 15. Model tests by shaking table

The movements of 4 kinds of stones with different shapes have been investigated under the earthquake conditions of 0, 200gal and 400gal sine wave of 3Hz. More than 10 times of repeated experiments have been carried out for each case. The following results have been obtained.

1. The movement distance for the case of a 400gal earthquake is 3.4 times longer than the case of no earthquake for the No.4 stone. Therefore, the effect of earthquake on the movement distance is very large.
2. The movement distance for the case of a 400gal earthquake is longer than the case of a 200gal earthquake. So it seems that the movement distance is proportional to the earthquake magnitude.
3. The shape of the falling stone has effect on the movement distance. The movement distance of the No. 5 stone is much smaller than that of No. 4. This is because that the earthquake can change the movement pattern and cause the rotation motion. It can be seen that the No. 5 stone has very sharp edges and vertices, which may stop its rotation movement (Fig. 16).

It should be noticed that it is difficult to distinguish the velocity obtained from *P*-phase because the model slope is too small and there are very few *P*-phase during the movements.

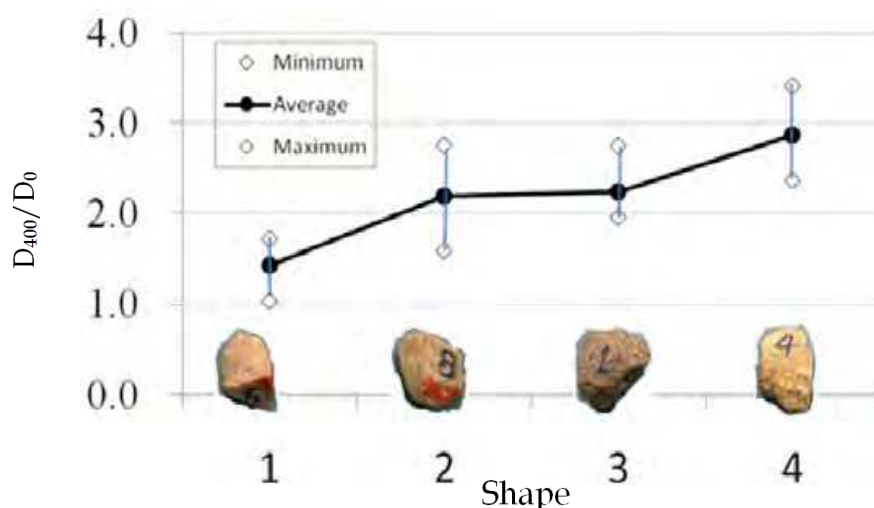


Fig. 16. Difference from shape of falling stone

4.4 Numerical simulation of landslide by using DDA

Simulation of landslide by using numerical methods is an effective way in order to overcome the dimension limit of the model test by using shaking table. In this study, Discontinue Deformation Analysis (DDA), developed by Shi and Goodman (Shi et al., 1984), is used since it is applicable to simulating the rigid body movements and large deformations of a rock block system under general loading and boundary conditions. Several extensions of the original DDA have been made in this study so that earthquake wave can be taken into the simulation for different ways.

Before simulating a real landslide, the applicability of the extended DDA has been verified by various simple models with theoretic solutions. For example, a simple model shown in Fig. 17 is calculated by both the theoretic solution and DDA simulation.

The theoretic solution of movement distance can be calculated by the following formula:

$$S_0 = \frac{1}{2}at^2 \quad (9)$$

where

$$\alpha = g[\sin \theta - (k \tan \phi_0) \cos \theta] \quad (10)$$

The results of the movement distance are in good agreement with each other as shown in Fig. 18.

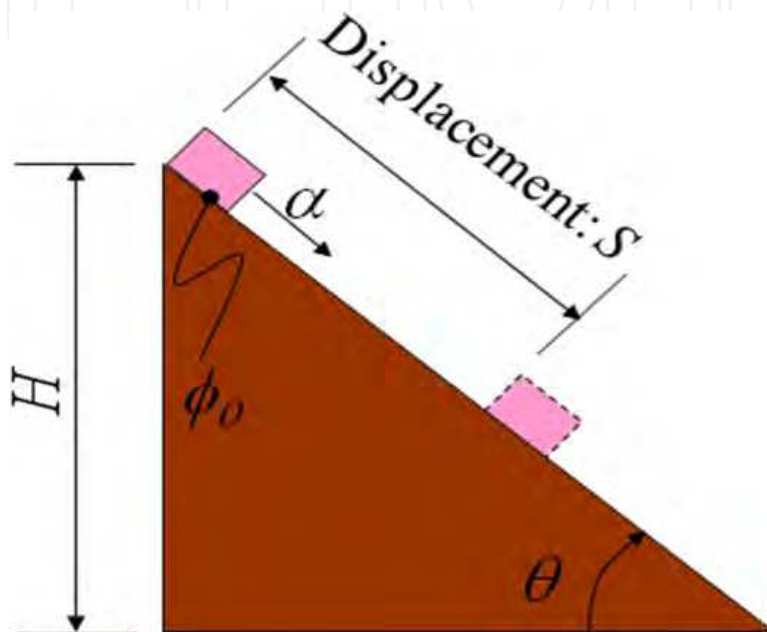


Fig. 17. The DDA model

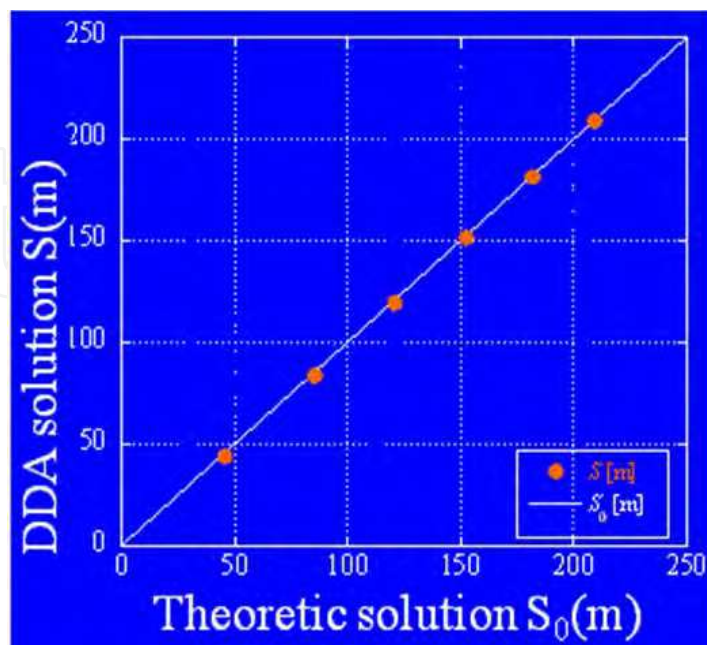


Fig. 18. The results

We applied the extended DDA to simulate the Dongheko landslide in Qingchuan prefecture. The vertical section shown in Fig. 19 is taken along the red line in Fig. 19. The DDA software and the model are shown in Fig. 20. The parameters for both the material and DDA program are also shown in Fig. 20.

Since the real earthquake curves are not available, a sine wave is used. The movements of debris at different times obtained from DDA simulation are shown in Fig. 21.

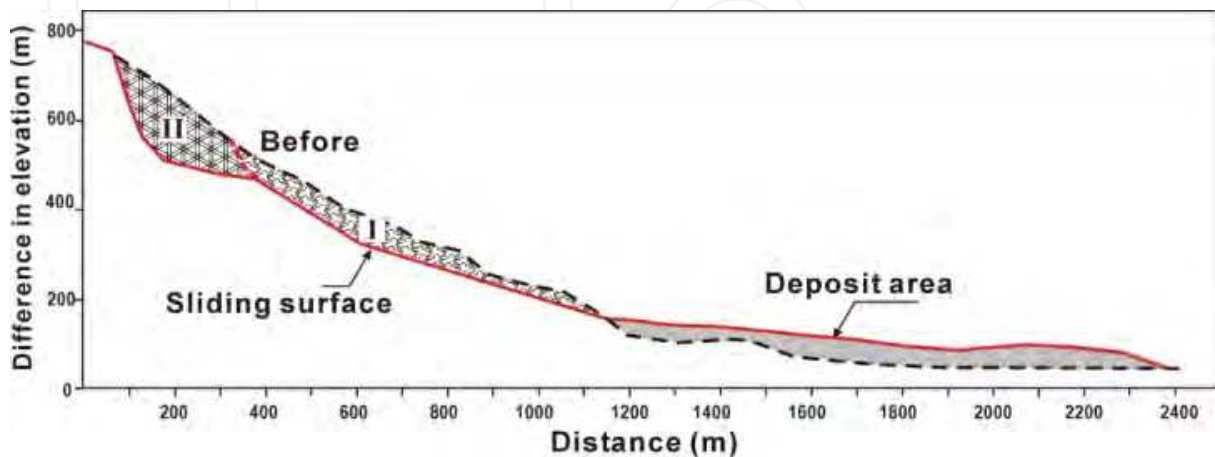


Fig. 19. Vertical section of the Dongheko landslide

It has been shown that an 800gal sine wave can cause long distance movements of debris like real one. The rotation and flying movements are the major reasons for long-distance movement, which can be easily observed in DDA simulations.

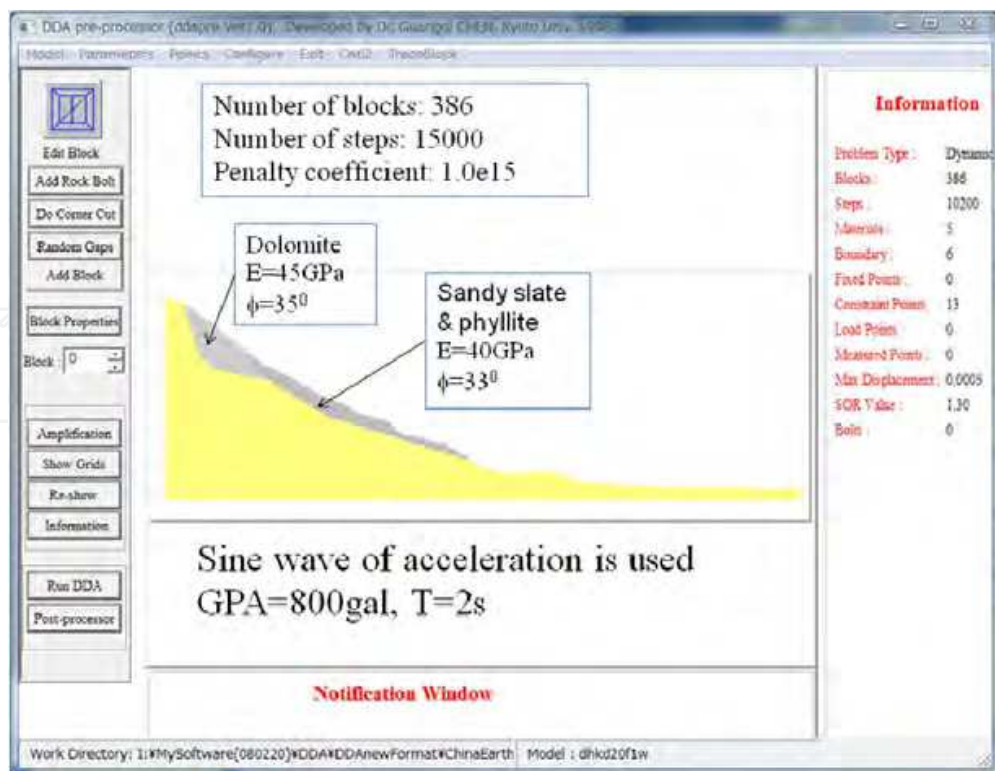


Fig. 20. DDA software developed by Chen and the model of Dongheko landslide

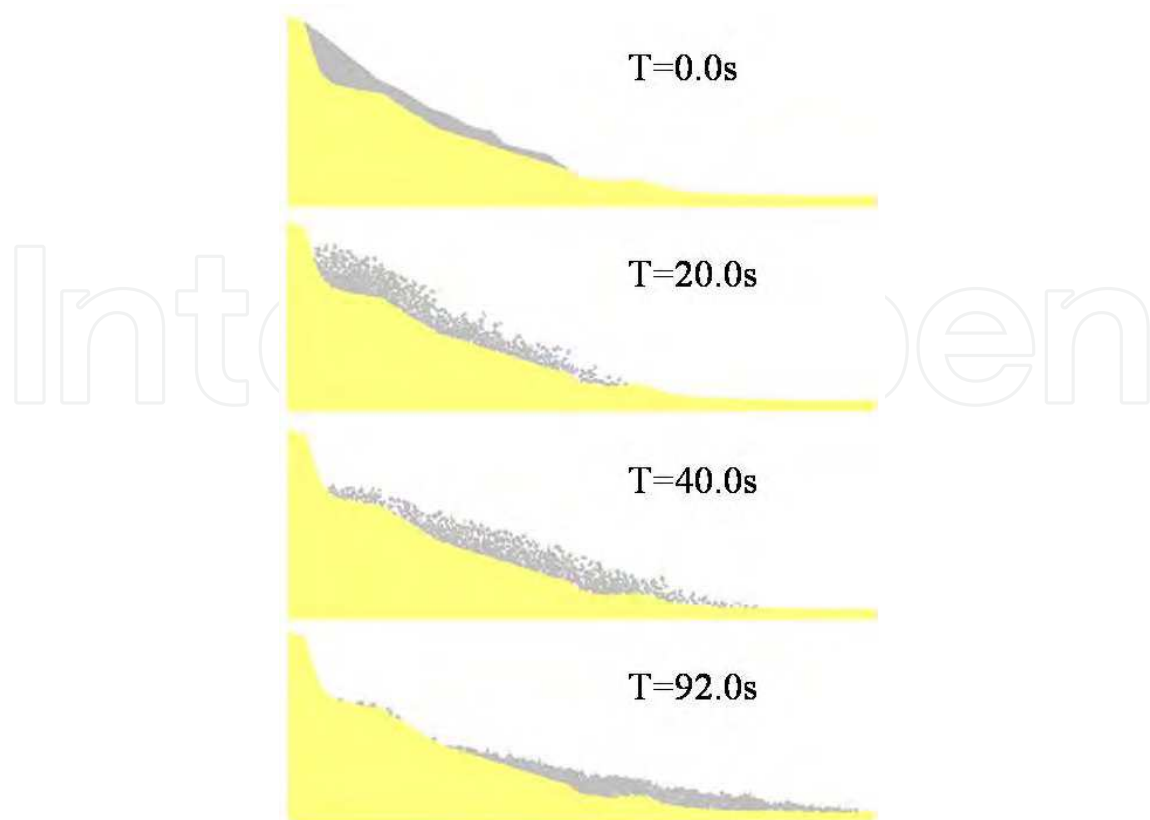


Fig. 21. The numeric simulation of debris movements by the extended DDA

5. Debris flow arising from the earthquake

Strong earthquakes not only trigger co-seismic landslides but also they affect subsequent rainfall-induced debris flows over a long term because these co-seismic landslides greatly increased the amount of sediment material for potential debris flows (Lin et al.,2006; Tang et al.,2009; Khattak et al.,2010). After the 2008 Wenchuan Earthquake, the earthquake affected areas experienced two rainy seasons till 2010, and a large number of debris flows occurred, which claimed as many as 450 fatalities. It makes the restoration and reconstruction much more difficult (Xie et al.,2008).

In this section, at first, the characteristics of debris flows in the earthquake affected areas are summarized. And then, an approach of simulating debris flow is proposed for disaster mitigation. Finally, a large scale debris flow is simulated so as to show the effectiveness of the proposed.

5.1 Characteristics of debris flow after the earthquake

1. Clear relation to the earthquake

A large number of debris flows occurred in the earthquake affected areas. For example, there are 46 debris flows found in Beichuan area. The distribution of these debris flows is shown in Fig. 22 in which the red line indicates the main fault of the quake, blue lines indicate rivers and the numbers indicate the locations of the debris flows. It can be seen that these debris flows are distributed along the rivers on the two sides of the earthquake fault. Therefore, the debris flows are highly related to the earthquake.

2. Large surge peak discharge and huge volume

Since the material sources of debris flow got much richer after earthquake, it is easy to form large scale debris flow. For example, the surge peak discharge reached $260 \text{ m}^3/\text{s}$ in the debris flow occurred in Beichuan town on Sept. 24, 2008. The volume was too large to a basin with the area of 1.54 km^2 . The cover of debris is so thick that it buried the fourth floor of some buildings. Another example is Sanyanyu debris flow. The volume of the debris reached 144.20 million m^3 . The debris flow carried many huge stones and destroyed houses and bridges (Tang et al., 2009).

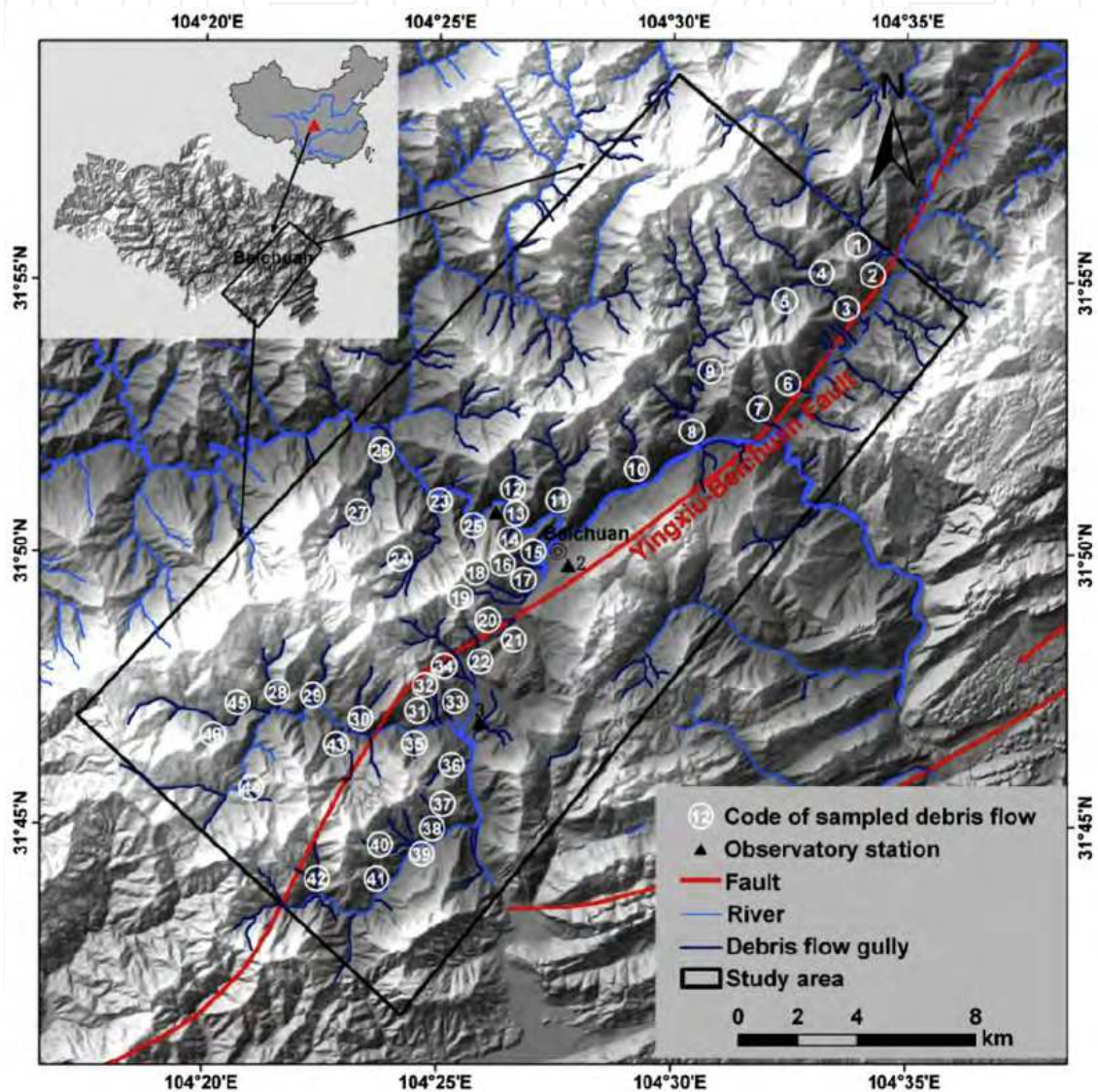


Fig. 22. 46 debris flows in the Beichuan area (Picture from Tangchuan et al., 2010)

Many preventive structures designed based on the standard of conventional debris flow were also destroyed by the large scale debris flows after the earthquakes. For example, 19 check dams were destroyed by the Wenjia debris flow occurred in Mianzhu Qingping town area on Aug. 13, 2010. The Fig. 23(a) shows one of the check dam destroyed by the debris flow. The extreme large scale and destructive impact of the debris flow seems beyond imagination.

3. The low critical precipitation for triggering debris flow

The critical precipitation for triggering debris flow got decreased obviously after the earthquake. For example, the critical precipitation of 37mm became lower after the earthquake in Zhouqu County areas. A 22mm rainfall could trigger a debris flow during the past 3 years. According to preliminary analysis by Tang et al. (2009), the critical cumulative precipitation has been reduced about 14.8%-22.1%, the critical rainfall intensity per hour about 25.4 % ~31.6% in Beichuan County area.



Fig. 23. (a): The destroyed check dam in Qingping debris flow; (b): Ming river blocked at Yingxiu town by Hongchungou debris flow (photographs from Tang chuan)

4. River blocking

The disasters chain induced by the earthquake is very significant. The earthquake induced landslides caused debris flows which blocked rivers, and flooding disasters occurred. For example, Jianjiang River was blocked at 3 locations and half blocked at 8 locations by debris flows during the rainstorm on Sept. 24, 2008. Mianyuan River was blocked at 2 locations and half blocked at 11 locations by debris flows occurred on Aug. 13, 2010. Ming River was blocked at 1 location and half blocked at 5 locations by debris flows occurred on Aug. 14, 2010 (see Fig. 23 (b)).

5.2 An approach of simulating debris flow

Many studies on debris flow focused on estimation of an alluvial fan for predicting debris flow inundation areas (Glade,2005;Berti and Simoni,2007). They can be divided into three categories: dynamic models, volume-based models and topographic based models. For the 2008 Wenchuan earthquake, an empirical formula of estimating alluvial fan has been presented by Tang et al. (2010) based on statistical analysis.

In this study, we propose an approach for numerical simulation of debris flow to analyze or predict the peak discharge and the volume of a debris flow and its inundation area. The approach consists of the following 5 procedures.

1. Identify the earthquake induced landslides

The earthquake induced landslides can be identified by RS technique using aerial photos and satellite imagines. The locations and the shapes of all the debris deposits in a drainage area should be obtained from this procedure.

2. Make field investigations.

The thicknesses of all the debris deposits and the geological and geotechnical behaviors should be investigated in this procedure.

3. Generate the grids using GIS.

Grids are required for solving equations with finite different method. A DEM map can be converted to a raster image using GIS for the drainage area. The grids can be obtained by saving the raster data.

4. Solve the equations.

The debris and water mixture is assumed to be a uniform continuous, incompressible, unsteady Newtonian fluid. The following Navier-Stokes equations are used for debris flow governing equations:

$$\begin{aligned} \nabla u &= 0 \\ \rho \frac{\partial u}{\partial t} + \rho u \cdot \nabla u &= \rho g - \nabla p + \mu \nabla^2 u \end{aligned} \tag{11}$$

where $u = (u, v, w)$ is velocity; ρ is the mass density; p is the pressure; μ is dynamic viscosity; $g = (0, 0, g)$, g is the gravitational constant and t is time.

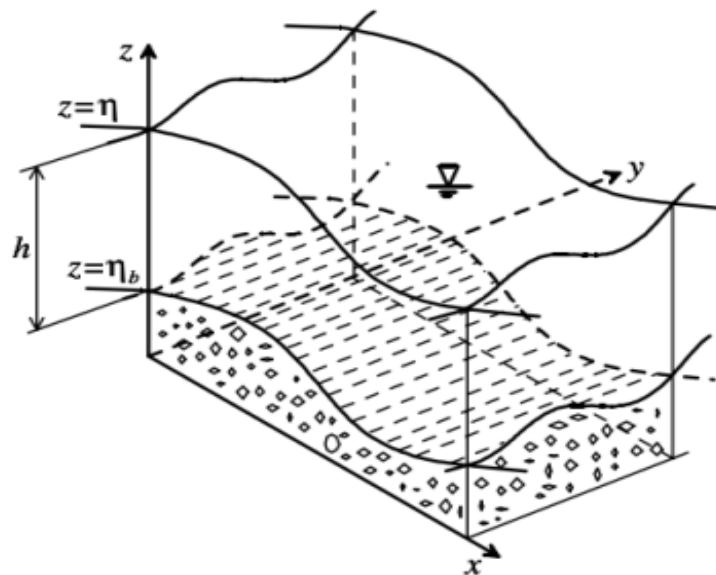


Fig. 24. Definition of coordinate system for 2D governing equations

The so-called depth-averaged model as shown in Fig. 24 is used. And then the following equations are used instead of Eq. (11). They are solved by finite difference method (FDM).

$$\frac{\partial h}{\partial t} + \frac{\partial M}{\partial x} + \frac{\partial N}{\partial y} = 0 \tag{12}$$

$$\frac{\partial M}{\partial t} + \alpha \frac{\partial(MU)}{\partial x} + \alpha \frac{\partial(MV)}{\partial y} = -\frac{\partial H}{\partial x} gh + \nu \beta \left(\frac{\partial^2 M}{\partial x^2} + \frac{\partial^2 M}{\partial y^2} \right) - gh \cos \theta_x \tan \xi \tag{13}$$

$$\frac{\partial N}{\partial t} + \alpha \frac{\partial(NU)}{\partial x} + \alpha \frac{\partial(NV)}{\partial y} = -\frac{\partial H}{\partial y} gh + \nu\beta\left(\frac{\partial^2 N}{\partial x^2} + \frac{\partial^2 M}{\partial y^2}\right) - gh \cos\theta_y \tan\xi \quad (14)$$

Where $M = Uh$ and $N = Vh$ are the x – and y – components of the flow flux; U and V are the x – and y – components of the depth-average velocity; H is the height of the free surface; h is the flow depth; θ_x and θ_y are the angle of inclination at the bed along the x and y directions, respectively; α and β are the momentum correction factors; $\nu = \mu / \rho_d$ is kinematic viscosity, ρ_d is the equivalent density of the debris mixture, and $\rho_d = \rho_s v_s + \rho_w v_w$, ρ_s and ρ_w are the densities of solid grains and water, v_s and v_w are the volumetric concentrations of solids particles and water in the mixture; and $\tan\xi$ is the dynamic friction coefficient.

5. Visualize the results

The results from FDM are converted to GIS layers. The maps of maximum surge peak discharge, velocity distribution and in inundation area can be made by GIS. Also the animation of debris flow can be easily made.

5.3 Numerical simulation of the Hongchungou debris flow

The proposed approach has been used to simulate the Hongchungou debris flow occurred in Hongchungou drainage area on August 14, 2010. The materials carried by the debris flow blocked Ming River just at a little upper side about 200m from Yingxiu town, the epicenter of the 2008 Wenchuan Earthquake (Fig. 25), . The road along the river became the new temporary river channel and water flowed into Yingxiu town. As the result, serious flood occurred in the newly reconstructed town. The disaster claimed 13 lives and 59 missing persons.

The distribution of the earthquake induced landslides has been identified by using RS with the aerial photographs taken by The Ministry of Land and Resources of China. The aerial photograph 0.3m resolution of Hongchungou area is shown in Fig. 26(a).

In this study, the object-based analysis (OBA) is adapted for image analysis unlike traditional spectral information based image analysis method since there exists the so-called ‘salt and pepper’ appearance in the output of the latter (Tapas R. Martha et al., 2010). The analysis includes the following steps.

1. The aerial photos are ortho-rectified based on the 20m DEM obtained from the China Geology Survey Bureau, in order to remove the distorting effects of tilt and terrain relief.
2. The image is divided into objects based on homogeneity of pixel values through edge-based segmentation algorithm (Kerle et al., 2009), since it is very fast and only one parameter is needed for scale level. Scale level 30 and merge level 93 are used for image segmentation.
3. NDVI index is used to separate vegetation from other objects. Spatial, spectral and texture attributes are separately computed for each object. Then, various land covers are classified based on user-defined training data, selected by combing with 3 dimensional image in order to improve the interpretation refinement;
4. The non-landslide objects are eliminated by the assumption that landslide will not occur for the slope gradient less than 5°.



Fig. 25. The blocked Ming River and new Yingxiu town in flood by Hongchungou debris flow.

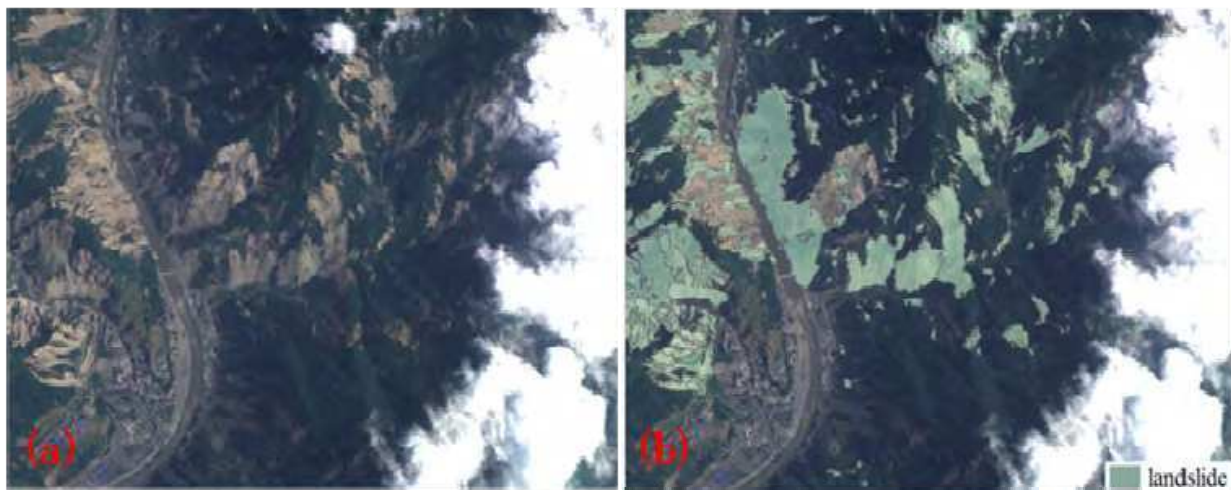


Fig. 26. (a): Aerial photography of Hongchun valley; (b): identified landslides in Hongchun valley

The obtained landslides are shown in Fig. 26(b). It can be seen that all the landslides were accurately recognized. There is not so-called 'salt and pepper' appearance.

Combining with field investigation, we finally selected four landslides: H1, H2, H3, H4 as the main loose source material of the debris flow (Fig. 27). The area of each landslide is 7,688 m² for H1, 5,137 m² for H2, 2,002 m² for H3, 4 4,567 m² for H4.

Since only a 20m DEM map is available for generating grids, the 4,000mX3,400m area is divided into 200X170 grids by using GIS. The rheological parameters are assumed constant (Tang et al., 2011a), and they are: $\rho_d = 2050 \text{ kg/m}^3$, $\alpha = 1.25$, $\beta = 1.0$, $\mu = 0.11$, $g = 9.8 \text{ m/s}^2$, $\tan \xi = 0.6$.

The results from FDM are converted to GIS layers for visualizing. The movements of the debris flow are illustrated in Fig. 28(a)-(d) for different time. It can be seen that the river is blocked in Fig. 28(d). The distribution of the maximum depth of the whole flow is shown in Fig. 28(e). According to the simulation results, the debris flow takes 150s to travel about 3,300 m along the valley with an average flow velocity of about 22m/s.

Comparing the simulated results with the actual event, we found that they are in good agreement with each other. Therefore, the proposed approach has been shown applicable and useful for predicting the movement of potential debris flow arising from earthquake.



Fig. 27. Identified landslides as loose material of the debris flow

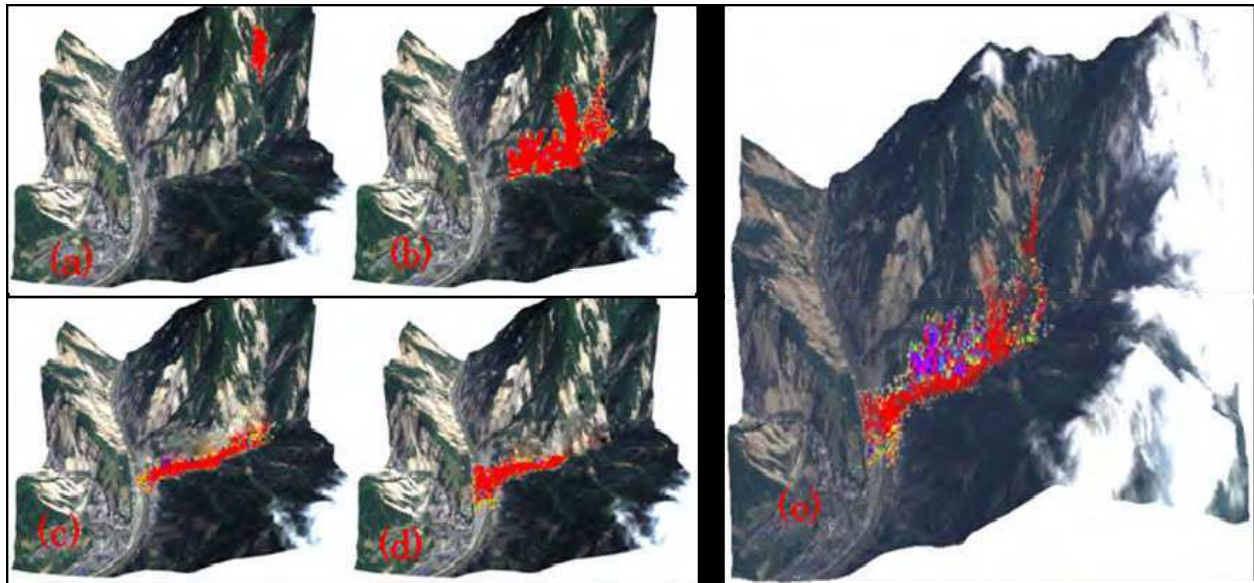


Fig. 28. The movement of the debris flow (a) for $t=10s$, (b) $t=76s$, (c) $t=120s$, (d) $t=150s$ and (e) for the distribution of the maximum depth of Hongchungou debris flow.

6. Conclusions

A strong earthquake can induce a chain of disasters. The disaster chain from the 2008 Wenchuan earthquake has been discussed.

The characteristics of the earthquake induced landslides have been summarized as follows.

1. A large number of landslides (56,000) were induced by the earthquake;
2. Large quantities of large-scale landslides (113) occurred and are listed in this chapter.

3. The landslides in the hanging wall are more than the footing wall and about 70% landslides are located in the region of 3km from the fault.
4. Large-scale landslide can occur at the locking segment of the rupture fault.
5. There is a clear relationship between the sliding direction of landslides and the fault strike.
6. Large quantities of long run-out landslides occurred and are listed in this chapter. Regression formulas of run-out distance have been obtained based on the areas and volumes of landslides.
7. A large number of landslide dams (34) were formed.

The susceptibility analysis of the earthquake induced landslides has been carried out by both statistical analysis and ANN analysis based on slope units rather than the traditional grids. The relationship of landslide distribution with individual causative factor has been investigated. It has been found that slope gradient, elevation, slope range, the distances to the fault, the distances to a stream have contributed to landslides while specific catchment area, slope aspect and lithology have no clear relationship. A susceptibility map has been made for analysis of the earthquake induced landslides in Qingchuan County.

A Multiplex Acceleration Model has been proposed for analysis of the long run-out mechanism based on trampoline effect. Table model tests and DDA simulation were carried out. It has been shown that the proposed Multiplex Acceleration Model is reasonable and applicable.

The earthquake induced landslides can easily form debris flows after the earthquake. The characteristics of the debris flows arising from the 2008 Wenchuan earthquake have been summarized as follows.

1. There is a clear relation to the earthquake according to the distribution of the debris flows along the earthquake fault.
2. Most of debris flows have large surge peak discharges and huge volumes.
3. The critical precipitation for triggering debris flow became lower.
4. Many rivers were blocked by the debris flows and serious damages have been caused by the debris dams.

An approach of simulating debris flow has been proposed. The earthquake induced landslides are identified by RS with object-based analysis method, which can overcome the problem of the so-called 'salt and pepper' appearance existed in the traditional spectral information based image analysis method. A practical simulation has been carried out and the proposed approach has been shown effective and useful for estimating the movement behaviours of a potential debris flow arising from a strong earthquake.

7. Acknowledgment

The presented research work and the preparation of this paper have received financial support from the Global Environment Research Found of Japan (S-8), Grants-in-Aid for Scientific Research (Scientific Research (B), 22310113, G. Chen) from JSPS (Japan Society for the Promotion of Science). These financial supports are gratefully acknowledged.

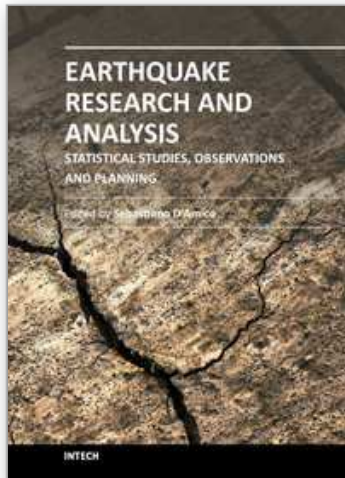
8. References

- Berti, M., Simoni, A. (2007). Prediction of debrisflow inundation areas using empirical mobility relationships. *Geomorphology*, Vol. 90, (October 2007), pp. 144-161

- Changa, KJ., Taboada, A., Linb, ML. & Chenc, RF. (2005). Analysis of landsliding by earthquake shaking using a block-on-slope thermo-mechanical model: Example of Jiufengershan landslide, central Taiwan. *Engineering Geology*, Vol. 80, (May 2000), pp. 151-163, ISSN 0013-7952
- Chigira, M. & Yagi, H. (2006). Geological and geomorphological characteristics of landslides triggered by the 2004 Mid Niigata prefecture earthquake in Japan. *Engineering Geology*. Vol. 82, No. 4, (February 2006), pp. 202-221, ISSN 0013-7952
- Cui, P., Zhu, Y., Han, Y., Chen, X. & Zhuang, J. (2009). The 12 May Wenchuan earthquake-induced landslide lakes: distribution and preliminary risk evaluation. *Landslides*, Vol. 6. No. 3, (June 2009), pp. 209-223, ISSN 1612-510X
- Dai, F., Xu, C., Yao, X., Xu, L., Tu, X. & Gong, Q. (2011). Spatial distribution of landslides triggered by the 2008 Ms 8.0 Wenchuan earthquake, China. *Journal of Asian Earth Sciences*, Vol. 40, No. 4, (March 2011), pp. 883-895, ISSN 1367-9120
- Dai, F.C., Lee, C.F. (2002). Landslide characteristics and slope instability modeling using GIS Lantau Island, Hong Kong. *Geomorphology* Vol. 42, (January 2002), pp. 213 - 238
- David, R. M. (2002). *Arc Hydro: GIS for Water Resources*, ESRI Press, Redlands, CA, US.
- Ermini, L., Catani, F., Casagli, N. (2005). Artificial neural networks applied to landslide susceptibility assessment. *Geomorphology* 66 (1 - 4), pp. 327 - 343
- Garrett, J. (1994) Where and why artificial neural networks are applicable in civil engineering, *Journal of Computing Civil Engineering* , Vol.8, No.2, pp. 129-130
- Glade, T., 2005. Linking debris-flow hazard assessments with geomorphology. *Geomorphology*, Vol. 66, pp. 189-213
- Gorum, T., Fan, X., Westen, C., Huang, R., Xu, Q., Tang, C. & Wang, G. (2011). Distribution pattern of earthquake-induced landslides triggered by the 12 May 2008 Wenchuan earthquake. *Geomorphology*, doi:10.1016/j.geomorph.2010.12.030, ISSN 0169-555X
- Huang, R., Pei, X., Fan, X., Zhang, W., Li, S. & Li, B. (2011a). The characteristics and failure mechanism of the largest landslide triggered by the Wenchuan earthquake, May 12, 2008, China. *Landslides*, (June 2011), doi:10.1007/s10346-011-0276-6, ISSN 1612-510X
- Huang, R., Xu, Q. & Huo, J. (2011b). Mechanism and geo-mechanics models of landslides triggered by 5.12 Wenchuan earthquake. *Journal of Mountain Science*, Vol. 8, No. 2, (April 2011), pp. 200-210, ISSN 1672-6316
- Jibson, R., Harp, E. & Michael, J. (2000). A method for producing digital probabilistic seismic landslide hazard maps. *Engineering Geology*, Vol. 58, No. 3-4, (December 2000), pp. 271-289, ISSN 0013-7952
- Keefer, D. (1984). Landslides caused by earthquakes. *Geological Society of America Bulletin*, Vol. 95, No. 4, (April 1984), pp. 406-421, ISSN 0016-7606
- Keefer, D. (2000). Statistical analysis of an earthquake-induced landslide distribution the 1989 Loma Prieta, California event. *Engineering Geology*, Vol. 58, No. 3, (December 2000), pp. 231-249, ISSN 0013-7952
- Keefer, D. (2002). Investigating landslides caused by earthquakes - A historical review. *Surveys in Geophysics*, Vol. 23, No. 6. (November 2002), pp. 473-510, ISSN 0169-3298
- Kerle, N., de Leeuw, J., (2009). Reviving legacy population maps with object-oriented image processing techniques. *IEEE Transactions on Geoscience and Remote Sensing*, Vol. 47, pp. 2392-2402

- Khattak G A, Owen L A, Kamp U, Harp E L. (2010). Evolution of earthquake-triggered landslides in the Kashmir Himalaya, northern Pakistan. *Geomorphology*, Vol. 115, pp. 102-108
- Khazai, B., Sitar, N., (2004). Evaluation of factors controlling earthquake-induced landslides caused by Chi-Chi earthquake and comparison with the Northridge and Loma Prieta events. *Engineering Geology*, Vol. 71, No. 1, (January 2004), pp. 79-95, ISSN 0013-7952
- Lee, C., Huang, C., Lee, J., Pan, K., Lin, M., Dong, J. (2008). Statistical approach to earthquake-induced landslide susceptibility. *Engineering Geology*, Vol. 100, No. 1, (June 2008), pp. 43-58, ISSN 0013-7952
- Lin, C.W., Liu, S.H., Lee, S.Y., Liu, C.C., (2006). Impacts of the Chi-Chi earthquake on subsequent rainfall induced landslides in central Taiwan. *Engineering Geology* 86, pp. 87-101
- Lin C W, Shieh C L, Yuan B D. (2003). Impact of Chi-Chi earthquake on the occurrence of landslides and debris flows: example from the Chenyulan River watershed, Nantou, Taiwan. *Engineering Geology*, Vol. 71, pp.49-61
- Miles, B. & Keefer, D. (2009). Evaluation of CAMEL - comprehensive areal model of earthquake-induced landslides. *Engineering Geology*, Vol. 104, No. 1, (February 2009), pp. 1-15, ISSN 0013-7952
- Nefeslioglu, H.A., Gokceoglu, C., Sonmez, H. (2008). An assessment on the use of logistic regression and artificial neural networks with different sampling strategies for the preparation of landslide susceptibility maps. *Engineering Geology*, Vol. 97, pp. 171 - 191
- Papadopoulos, G. & Plessa, A. (2000). Magnitude-distance relations for earthquake-induced landslides in Greece. *Engineering Geology*, Vol. 58, No. 4, (December 2000), pp. 377-386, ISSN 0013-7952
- Pradhan.B, S.Lee. (2010). Landslide susceptibility assessment and factor effect analysis: backpropagation artificial neural networks and their comparison with frequency ratio and bivariate logistic regression modeling. *Environmental Modelling & Software*, Vol. 25, pp. 747 - 759
- Qi, S., Xu, Q., Lan, H., Zhang, B. & Liu, J. (2010). Spatial distribution analysis of landslides triggered by 2008.5.12 Wenchuan Earthquake, China. *Engineering Geology*, Vol. 116, No. 2, (August 2010), pp. 95-108, ISSN 0013-7952
- Qi, S., Xu, Q., Zhang, B., Zhou, Y., Lan, H. & Li, L. (2011). Source characteristics of long runout rock avalanches triggered by the 2008 Wenchuan earthquake, China. *Journal of Asian Earth Sciences*, Vol. 40, pp: 896-906, ISSN 1367-9120
- Rodriguez, C., Bommer, J. & Chandler, R. (1999). Earthquake-induced landslides: 1980-1997. *Soil Dynamic and Earthquake Engineering*, Vol. 18, No. 5, (March 1999), pp. 325-346, ISSN 0267-7261
- S.Lee, D. G. Evangelista. (2006). Earthquake-induced landslide-susceptibility mapping using an artificial neural network", *Nat. Hazards Earth Syst. Sci.*, Vol. 6, pp. 687-695
- Shaller, P.J. & Shaller, A.S. (2006). Review of proposed mechanisms for sturzstroms (long runout landslides). *Sturzstroms and Detachment Faults*, Anza-Borrego State Park, California, pp.185-202
- Tang C, Zhu J, Li W L. (2009) Rainfall triggered debris flows after Wenchuan earthquake. *Bull Eng Geol Environ*, Vol. 68, pp. 187-194

- Tang C, Ding J, Qi X. (2010). Remote sensing dynamic analysis of rainstorm landslide activity in Wenchuan high-intensity earthquake area. *China university of geosciences journal*, Vol.35, pp. 317-323
- Tang C, Zhu J, Qi X. (2011a). Landslide Hazard Assessment of the 2008 Wenchuan Earthquake: a case study in Beichuan Area. *Canadian Geotechnical Journal*. Vol. 48, pp. 128-145
- Tang, C., Zhu, J., Qi, X. & Ding, J. (2011b). Landslides induced by the Wenchuan earthquake and the subsequent strong rainfall event: A case study in the Beichuan area of China. *Engineering Geology*, doi:10.1016/j.enggeo.2011.03.013, ISSN 0013-7952
- Tapas R. Martha, Norman Kerle, Victor Jetten, Cees J. van Westen, K. Vinod Kumar. (2010). Characterising spectral, spatial and morphometric properties of landslides for semi-automatic detection using object-oriented methods. *Geomorphology* Vol. 116, PP. 24-36
- Wu, S., Wang, T., Shi, L., Sun, P., Shi, J., Li, B., Xin, P. & Wang, H. (2010). Study on catastrophic landslides triggered by 2008 great Wenchuan earthquake, Sichuan, China. *Journal of Engineering Geology*, Vol. 18, No. 2, pp. 145-159, ISSN 1004-9665 (in chinese)
- Xie, H., Zhong, D.L., Jiao, Z., et al. 2008. Debrisflow in Wenchuan quake-hit area in 2008. *Journal of Mountain Science* 27(4), 501-509.
- Xu, Q., Pei, X., Huang, R. et al. (2009a). *Large-scale Landslides Induced by the Wenchuan earthquake*, Science Press, ISBN 978-7-03-026906-5, Beijing, China (in chinese)
- Xu, Q., Fan, X., Huang, R. & Westen, C. (2009b). Landslide dams triggered by the Wenchuan earthquake, Sichuan Province, south west China. *Bulletin of Engineering Geology and the Environment*, Vol. 68, No. 3, (August 2009), pp. 373-386, ISSN 1435-9529
- Yagi, H., Sato, G., Higaki, D., Yamamoto, M. & Yamasaki, T. (2009). Distribution and characteristics of landslides induced by the Iwate-Miyagi Nairiku Earthquake in 2008 in Tohoku District, Northeast Japan. *Landslides*, Vol. 6, No. 4, (December 2009), pp. 335-344, ISSN 1612-510X
- Yin, J., Chen, J., Xu, X., Wang, X. & Zheng, Y. (2010). The characteristics of the landslides triggered by the Wenchuan Ms 8.0 earthquake from Anxian to Beichuan. *Journal of Asian Earth Sciences*, Vol. 37, No. 6, (March 2010), pp. 452-459, ISSN 1367-9120
- Yin, Y., Wang, F. & Sun, P. (2009a). Landslide hazards triggered by the 2008 Wenchuan earthquake, Sichuan, China. *Landslides*, Vol. 6, No. 2, (June 2009), pp. 139-151, ISSN 1612-510X
- Yin, Y. (2009b). Rapid and long run-out features of landslides triggered by the Wenchuan Earthquake. *Journal. of Engineering. Geology*, Vol. 17, pp. 153-166 (in Chinese)



**Earthquake Research and Analysis - Statistical Studies,
Observations and Planning**

Edited by Dr Sebastiano D'Amico

ISBN 978-953-51-0134-5

Hard cover, 460 pages

Publisher InTech

Published online 02, March, 2012

Published in print edition March, 2012

The study of earthquakes plays a key role in order to minimize human and material losses when they inevitably occur. Chapters in this book will be devoted to various aspects of earthquake research and analysis. The different sections present in the book span from statistical seismology studies, the latest techniques and advances on earthquake precursors and forecasting, as well as, new methods for early detection, data acquisition and interpretation. The topics are tackled from theoretical advances to practical applications.

How to reference

In order to correctly reference this scholarly work, feel free to copy and paste the following:

Guangqi Chen, Yange Li, Yingbin Zhang and Jian Wu (2012). Earthquake Induced a Chain Disasters, Earthquake Research and Analysis - Statistical Studies, Observations and Planning, Dr Sebastiano D'Amico (Ed.), ISBN: 978-953-51-0134-5, InTech, Available from: <http://www.intechopen.com/books/earthquake-research-and-analysis-statistical-studies-observations-and-planning/earthquake-induced-a-chain-disasters->

INTECH
open science | open minds

InTech Europe

University Campus STeP Ri
Slavka Krautzeka 83/A
51000 Rijeka, Croatia
Phone: +385 (51) 770 447
Fax: +385 (51) 686 166
www.intechopen.com

InTech China

Unit 405, Office Block, Hotel Equatorial Shanghai
No.65, Yan An Road (West), Shanghai, 200040, China
中国上海市延安西路65号上海国际贵都大饭店办公楼405单元
Phone: +86-21-62489820
Fax: +86-21-62489821

© 2012 The Author(s). Licensee IntechOpen. This is an open access article distributed under the terms of the [Creative Commons Attribution 3.0 License](#), which permits unrestricted use, distribution, and reproduction in any medium, provided the original work is properly cited.

IntechOpen

IntechOpen